의학박사 학위논문

# Alleviation of Liver Fibrosis by Natural Killer Cell Therapy Through Suppressing Inflammation and Extracellular Matrix-Related Genes in a Liver Cirrhosis Mouse Model

# 간경변 마우스 모델에서 염증과 세포외기질 관련 유전자 억제를 통한 자연살해세포 치료의 간섬유화 완화

2023 년 8 월

서울대학교 대학원

의과학과 의과학전공

오 호 림

Ph.D. Dissertation of Philosophy

# 간경변 마우스 모델에서 염증과 세포외기질 관련 유전자 억제를 통한 자연살해세포 치료의 간섬유화 완화

# Alleviation of Liver Fibrosis by Natural Killer Cell Therapy Through Suppressing Inflammation and Extracellular Matrix-Related Genes in a Liver Cirrhosis Mouse Model

August 2023

Graduate School of Medicine

Seoul National University

Biomedical sciences

Ho Rim Oh

# 간경변 마우스 모델에서
# 염증과 세포외기질 관련 유전자 억제를 통한
# 자연살해세포 치료의 간섬유화 완화

지도 교수 강 건 욱

이 논문을 의학박사 학위논문으로 제출함

2023 년 4 월


서울대학교 대학원

의과학과 의과학전공

오 호 림


오호림의 의학박사 학위논문을 인준함

2023 년 6 월

위 원 장 _____ (인)

부위원장 _____ (인)

위 원 _____ (인)

위 원 _____ (인)

위 원 _____ (인)

# Alleviation of Liver Fibrosis by Natural Killer Cell Therapy Through Suppressing Inflammation and Extracellular Matrix–Related Genes in a Liver Cirrhosis Mouse Model

by Ho Rim Oh

Submitting a Ph.D. Dissertation of Philosophy

April, 2023

Confirming the Ph.D. Dissertation written by

Ho Rim Oh

June, 2023

Chair _____ (Seal)

Vice Chair _____ (Seal)

Examiner _____ (Seal)

Examiner _____ (Seal)

Examiner _____ (Seal)

# Abstract

Chronic liver disease can lead to liver fibrosis, cirrhosis and/or hepatocellular carcinoma (HCC), which are one of the major causes of morbidity and mortality worldwide. Activated hepatic stellate cells (HSCs) that lead to produce excessive extracellular matrix including collagen play a detrimental role in liver fibrosis progression. Natural killer cells (NK cells) perform the function of selectively recognizing abnormal or transformed cells through receptor activation and inducing target cell death. Considering that hepatic NK cells are lymphocytes abundant in the liver and play a direct role in killing target cells, the role of NK cells was investigated in the progression of liver cirrhosis in a preclinical carbon tetrachloride ($CCl_4$)-induced liver cirrhosis mouse model.

In this study, we examined the therapeutic effects of NK cells in the $CCl_4$-induced liver cirrhosis mouse model. NK cells were isolated from the spleen and expanded in a culture medium stimulated with cytokines. The expansion process resulted in a significant increase in NK cells expressing the natural killer group 2, member D (NKG2D) receptor. Intravenous injection of these NK cells effectively ameliorated liver cirrhosis by reducing inflammation, activation of HSC markers, and infiltration of

macrophages. To track the NK cells *in vivo*, luciferase-expressing NK cells were isolated and expanded from codon-optimized luciferase-expressing transgenic mice and administered to the cirrhosis mouse model. Bioluminescence imaging elucidated increased accumulation of the injected NK cells in the cirrhotic liver.

Transcriptomic analysis using QuantSeq 3' mRNA sequencing identified 33 downregulated genes related to the extracellular matrix (ECM) and 41 downregulated genes involved in the inflammatory response in the cirrhotic liver tissues treated with NK cells from the 1532 differentially expressed genes (DEGs). This finding suggested that repetitive administration of NK cells alleviated liver fibrosis via anti-fibrotic and anti-inflammatory mechanisms. Taken together, this research demonstrated that NK cells could have therapeutic effects in a $CCl_4$-induced liver cirrhosis mouse model, highlighting the ECM genes and inflammatory response genes as potential targets for intervention.

**Keyword :** liver cirrhosis; carbon tetrachloride ($CCl_4$); natural killer (NK) cells; bioluminescence imaging (BLI)

**Student Number :** 2016-21996

# Contents

Abstract ..... i

Contents ..... iii

List of Figures and Tables ..... iv

List of Abbreviation ..... vi

Introduction ..... 1

Material and Methods ..... 6

Results ..... 15

Discussion ..... 56

References ..... 68

Abstract in Korean ..... 80

# List of Figures and Tables

**Figure 1.** Schematic time course of natural killer (NK) cell isolation and expansion

**Figure 2.** Flow cytometric analysis of the isolated and expanded NK cell population

**Figure 3.** Validation of the expanded NK cell population

**Figure 4.** Evaluation of the $CCl_4$-induced liver cirrhosis mouse model

**Figure 5.** Reduced liver cirrhosis progression after NK cell transplantation in the $CCl_4$-induced liver cirrhosis mouse model

**Figure 6.** Decrease in fibrosis after NK cell transplantation in the $CCl_4$-induced liver cirrhosis mouse model

**Figure 7.** Schematic time course of $CCl_4$ treatment and bioluminescence imaging (BLI) for NK cell tracking

**Figure 8.** *In vitro* bioluminescence assay of splenocytes and expanded NK cells from codon-optimized luciferase transgenic mice

**Figure 9.** *In vivo* bioluminescence tracking of NK cells in the $CCl_4$-induced liver cirrhosis mouse model

**Figure 10.** QuantSeq analysis of treatment-dependent differentially expressed genes (DEGs)

**Figure 11.** Validation of expression levels of DEGs associated with extracellular matrix by qRT-PCR

**Figure 12.** Validation of expression levels of DEGs associated with inflammatory response by qRT-PCR

**Figure 13.** Schematic summary of NK cell therapeutics in $CCl_4$-induced liver cirrhosis mouse model in this study

**Table 1.** Target gene primer sequence

**Table 2.** Expression levels of DEGs involved in the extracellular matrix

**Table 3.** Expression levels of DEGs involved in the inflammatory response

# List of Abbreviation

| | |
|---|---|
| HSC | Hepatic stellate cell |
| NK cell | Natural killer cell |
| $CCl_4$ | Carbon tetrachloride |
| NKG2D | Natural killer group 2, member D |
| ECM | Extracellular matrix |
| DEGs | Differentially expressed genes |
| BLI | Bioluminescence imaging |
| MSC | Mesenchymal stem cell |
| PET | Positron emission tomography |
| SPECT | Single photon emission computed tomography |
| MRI | Magnetic resonance imaging |
| IFN-$\gamma$ | Interferon-$\gamma$ |
| TGF-$\beta$ | Transforming growth factor-beta |
| $\alpha$-SMA | Alpha-smooth muscle actin |
| GAPDH | Glyceraldehyde 3-phosphate dehydrogenase |
| SD | Standard deviation |
| MMP | Matrix metalloproteinase |
| IL | Interleukin |
| TNF | Tumor necrosis factor |

# Introduction

Liver cirrhosis is a chronic end-stage liver disease accompanied by scarring tissues resulting from various causes such as hepatitis, alcohol abuse, fatty liver, and drugs. Histologically, liver cirrhosis is characterized by diffuse nodular regeneration, fibrogenesis/fibrosis, and a collapse of the liver structure [1, 2]. The chronic inflammatory environment of the liver tissue triggers fibrotic liver tissue formation with persistent liver damage after activation of hepatic stellate cells (HSCs) [3]. Activated HSCs are one of the main components in the pathogenesis of liver fibrosis, cirrhosis, and hepatocellular carcinoma. HSCs are quiescent in the normal liver but can be activated during liver damage to a proliferative state with a myofibroblast phenotype with migratory and invasive capabilities [4-6].

At the clinical level, patients with decompensated liver cirrhosis have a poor prognosis [7]. Although various medications can be used to reduce the temporal symptoms of liver cirrhosis [7, 8], its most definitive treatment is transplantation. However, the transplantation procedure is complicated, and it is difficult to find a suitable donor.

At the preclinical level, a mouse model of liver cirrhosis can be

established by the hepatotoxicity of carbon tetrachloride ($CCl_4$)-induced free radicals. $CCl_4$ is used to dissolve non-polar compounds, such as fats and oils, and is activated by hepatic cytochrome P450 enzymes to form trichloromethyl and trichloromethyl-peroxy radicals in the body [9, 10]. These free radicals induce nucleic acid mutations and lipid peroxidation and destruct polyunsaturated fatty acids, leading to hepatotoxicity, inflammation, fibrosis, cirrhosis, and hepatocellular carcinoma [9, 10].

Cell therapy can be one treatment option for liver cirrhosis. Mesenchymal stem cells (MSCs) can reduce inflammation and apoptosis, increase hepatocyte regeneration, and improve liver function by regressing liver fibrosis [11]. In particular, MSCs can migrate to the liver and differentiate into hepatocytes during liver damage [12]. However, the role of specific cell types in MSCs is still poorly understood, and their side effects including promoting tumor growth are serious concerns [13].

Natural killer cells (NK cells) perform the function of selectively recognizing abnormal or transformed cells through receptor activation and inducing target cell death. NK cells that are important for host defense and memory-like responses could also contribute to treating liver cirrhosis [14-17]. Liver-resident NK cells showed protective effects in a $CCl_4$-induced liver cirrhosis mouse model

and could specifically kill activated HSCs but not quiescent HSCs [18–20]. Also, NK cells could negatively regulate HSCs in liver cirrhosis progression [21–24]. Considering that hepatic NK cells play a direct role in killing target cells, it was investigated that the role of NK cells in the progression of liver cirrhosis in a preclinical $CCl_4$–induced liver cirrhosis mouse model.

To further investigate the role of NK cells in liver cirrhosis, it is essential to isolate and expand these cells for in–depth studies. The spleen, the largest secondary lymphoid organ, contains red blood cells and immune cells, including NK cells, which could be one option for purifying NK cells. However, the frequency of NK cells in the spleen of a normal 2–3–month–old C57BL/6J mouse was reported to be only about 3~4% [25]. Therefore, the efficient isolation, extraction, and expansion of NK cells are important, providing the opportunity to elucidate the role of NK cells in liver cirrhosis.

Immune cells can migrate to specific locations to implement an appropriate host defense immune response. Therefore, tracking immune cells would provide critical evidence for their role. In this context, imaging techniques represent a great choice to track cells, and, in particular, reporter gene imaging can be a powerful tool to track and visualize cells *in vivo* [26]. A variety of imaging

techniques, including fluorescence, bioluminescence, positron emission tomography (PET), single photon emission computed tomography (SPECT), and magnetic resonance imaging (MRI), can be used for tracking cells. Among them, bioluminescence imaging (BLI) is a noninvasive visualization method that can be used in various fields of *in vitro* and *in vivo* biology due to the advantages of high sensitivity, resolution, and selectivity with a low background signal and a lack of external light excitation [26]. In the case of PET or SPECT, radioactive isotope labeling is required for cell tracking, and validation of changes in cell properties may be necessary during the labeling process [27]. In the case of an MRI, since the labeling of a contrast agent such as iron oxide is also required, it is necessary to validate that there is no change in cell characteristics during the labeling process [26, 27].

In this study, the delivery of NK cells—generated by a specific isolation and effective expansion method—to a recipient mouse with liver cirrhosis effectively ameliorated the progression of liver cirrhosis by reducing inflammation, HSC activation, and macrophage infiltration. The accumulation of therapeutic NK cells in the cirrhotic livers of mice using the BLI technique was observed. Therapeutic NK cells were prepared from the spleens of codon-optimized luciferase-expressing transgenic mice [28] and transferred to mice

with $CCl_4$-induced liver cirrhosis for visualization. RNA sequencing, a powerful technology that enables comprehensive gene expression analysis at the transcription level using next-generation sequencing technology [29, 30] was performed in this study. Subsequently, the transcriptomes of normal and cirrhosis-induced liver tissues by QuantSeq 3′ mRNA sequencing were investigated after treatment with NK cells.

# Materials and Methods

*Animals*

Experiments were approved by the Institutional Animal Care and Use Committee of the Seoul National University and Seoul National University Hospital (SNU-220113-5, IACUC No. 21-0034-S1A0). Mice were housed at room temperature with 40% to 60% humidity and fed standard a chow diet and water *ad libitum* in a 12 hours' light/dark cycle. Mice were tested for experiments after at least one week of acclimatization.

*Isolation and Expansion of NK cells*

Seven-week-old male BALB/c mice (n = 10) were killed by cervical dislocation, and spleens were removed and crushed to obtain splenocytes. NK cells were isolated from splenocytes by negative selection using an NK cell isolation kit (130-115-818, Miltenyi Biotec, Bergisch Gladbach, North Phine-Westphalia, Germany) according to the manufacturer's instructions [31]. Isolated NK cells were cultured at a density of $5 \times 10^6$ cells/mL in T-25 flasks in Roswell Park Memorial Institute-1640 medium (Cytiva, Marlborough, MA, USA) supplemented with 10% fetal bovine serum (FBS) (Gibco, Waltham, MA, USA), 1% L-glutamine

(Gibco), 1% Antibiotic-Antimycotic (Gibco), 50 μM β-mercaptoethanol (Sigma-Aldrich, St. Louis, MO, USA) and 50 ng/mL recombinant human IL-15 protein (R&D systems, Minneapolis, MN, USA). Fresh medium was added to the cells on days 4, 5, and 6. Cells were maintained in a humidified atmosphere containing 5% $CO_2$ and 95% air at 37℃.

*Fluorescence-Activated Cell Sorting (FACS)*

Cells were suspended in 1X PBS supplemented with 0.1% FBS. Cells were washed once in buffer and stained for 30 minutes with PE-conjugated anti-NKG2D, FITC-conjugated anti-CD3e, APC-conjugated anti-NKp46, and anti-CD19 (Biolegend, San Diego, CA, USA). After harvesting the cells, the expression of proteins was analyzed using NovoCyte flow cytometry (Agilent Technologies, Santa Clara, CA, USA) on over 10,000 cells.

*Interferon-γ (IFN-γ) ELISA*

IFN-γ cytokine was measured by the enzyme-linked immunosorbent assay (ELISA) (SIF50C, R&D systems) using the supernatant from the NK cells in 96-well U-bottom plate. Briefly, diluent assay solution was added to the collected supernatant (100 μL each) in a well of an ELISA plate and incubated for 2 hours at

room temperature. Plates were then washed and incubated with INF-$\gamma$ conjugate (200 $\mu$L/well) for 2 hours at room temperature. The reaction was then washed and incubated with substrate solution (200 $\mu$L/well) for 30 minutes at room temperature. Finally, the reaction was quenched with 50 $\mu$L of stop solution. The amount of antibody was measured in a Victor Nivo 3 (PerkinElmer, Waltham, MA, USA).

*$CCl_4$-Induced Liver Cirrhosis in Mice*

Seven-week-old male BALB/c mice were administered intraperitoneally with mineral oil (control, n = 4) or $CCl_4$ (1.5 mL/kg, diluted 1:3 in mineral oil, n = 4) twice a week for 3 weeks for validation of $CCl_4$-induced liver cirrhosis mouse model [32] and once a week from the 4th week (totaling 8 weeks) for NK cell therapeutics. NK cells were injected intravenously once a week from the 4th week after $CCl_4$ injection.

*Analysis of Fibrosis*

The area of liver fibrosis was quantified with Sirius red-stained slides. Paraffin-embedded liver tissues sliced and transferred to glass slides were deparaffinized and rehydrated. The slides were treated with Picro Sirius red solution (Abcam, Cambridge, UK) for

60 minutes and rinsed twice with 0.1% acetic acid solution and then with absolute alcohol. Slides were washed with distilled water, mounted, and scanned using the Olympus BX43 optical microscope with a CCD camera (Olympus, Tokyo, Japan). Red areas, considered fibrotic areas, were assessed by computer-assisted image analysis using MetaMorph software 7.8.10 (Universal Imaging Corporation, Bedford Hills, NY, USA) at 40× magnification. The average value of 6 randomly selected areas per sample was used as the percent area of fibrosis.

*Immunohistochemistry*

Slides of paraffin-embedded liver tissue sections were deparaffinized and rehydrated. After washing, the slides were boiled with 10 mM sodium citrate (pH 6.0) (ICN biomedicals, Costa Mesa, CA, USA) for antigen retrieval and then treated with 0.5% Triton X-100 (Yakuri pure chemicals, Kyoto, Japan) in Tris-buffered saline (TBS) for 5 minutes to permeabilize for antibodies.

Antibodies against transforming growth factor-beta (TGF-$\beta$) 1 (1:50 dilution, ab92486, Abcam), alpha-smooth muscle actin ($\alpha$-SMA) (1:100 dilution, ab7817, Abcam), and F4/80 (1:100 dilution, ab6640, Abcam) were diluted with TBS containing 1% BSA and applied overnight at 4℃. Next, the slides were incubated with

secondary antibodies of donkey anti-rat IgG Alexa Fluor 488 (1:500 dilution, A-21208, Thermofisher Scientific, Waltham, MA, USA), goat anti-mouse IgG Alexa Fluor 488 (1:500 dilution, A-11001, Thermofisher Scientific), and donkey anti-rabbit IgG Alexa Fluor 555 (1:500 dilution, A-31572, Thermofisher Scientific) for 1 hour. Finally, the slides were DAPI stained and mounted.

For H&E staining, the slides were deparaffinized, rehydrated, and treated with Mayer's hematoxylin (Agilent Technologies) for 20 seconds and washed. Next, eosin solution (Sigma-Aldrich) was added to the slides for 30 seconds and washed. Finally, the slides were mounted.

*Tracking of Therapeutic NK Cells in a Mouse Model with $CCl_4$-Induced Liver Cirrhosis*

For NK cell tracking experiments, five-month-old male C57BL/6 albino mice were administered mineral oil (control, n = 2) or $CCl_4$ (1.5 mL/kg, diluted in mineral oil, n = 3) twice a week for 3 weeks. NK cells from codon-optimized luciferase (luc)-expressing transgenic mice were isolated and expanded [28]. After inoculation of NK-luc cells ($1 \times 10^7$ cells/mouse, intravenous injection) into syngeneic albino mice, D-luciferin (3 mg/mouse) (Promega, Madison, WI, USA) was injected intraperitoneally as a substrate,

and *in vivo* bioluminescence images were acquired using the IVIS Lumina II (PerkinElmer).

*QuantSeq 3′ mRNA Sequencing*

Total RNA was isolated using the TRI Reagent solution (Invitrogen, Waltham, MA, USA). RNA quality was evaluated using 2100 Bioanalyzer with RNA 6000 Nano Chip (Agilent Technologies), and RNA quantification was determined using ND-2000 spectrophotometer (Thermofisher Scientific). Control and test RNA libraries were constructed following the manufacturer's instructions using QuantSeq 3′ mRNA-Seq library prep kit (Lexogen, Vienna, Austria). Briefly, 500 ng of total RNA was prepared, and an oligo-deoxythymidine (oligo-dT) primer containing an Illumina compatible sequence at the 5′ end was hybridized to the RNA and reverse transcribed. After degradation of the template RNA, second-strand synthesis was performed using random primers containing an Illumina-compatible linker sequence at the 5′ end. The double-stranded library was purified by using magnetic beads from reaction mixtures. Complete adapter sequences were added through an amplification process to generate clusters, and the completed library was purified from the reaction mixture. High-throughput sequencing was performed as single-end 75 sequencing

using NextSeq 500 (Illumina, San Diego, CA, USA).

*Gene Expression Data Analysis*

QuantSeq 3′ mRNA-Seq reads were aligned using Bowtie2 [33]. The alignment file was used for transcript assembly, abundance estimation, and differential expression of genes (DEGs) detection. DEGs were determined based on counts from unique and multiple alignments using coverage in BEDTools [34].

*RNA Isolation and Quantitative Real-Time PCR (qRT-PCR)*

Total RNA was extracted from cell lysates using TRI Reagent solution (Invitrogen). First-strand cDNA was synthesized from 1 $\mu$g of total RNA using the TOPscript cDNA synthesis kit (EZ005S, Enzynomics, Daejeon, Korea) according to manufacturer's instructions. Primer sequences are provided in Table 1. Quant Studio 5 Real-time PCR system (Applied Biosystems, Waltham, MA, USA) was utilized for cDNA amplification with Power SYBR® Green Master Mix (Applied Biosystems) under the following conditions: 95℃ for 10 minutes, followed by 45 cycles of 95℃ for 15 seconds and 61℃ for 1 minute. Expression levels of target mRNAs were analyzed using the ΔΔCt method and were normalized to expression levels of glyceraldehyde 3-phosphate dehydrogenase (GAPDH), a

housekeeping gene used as an endogenous control. The fold changes were expressed relative to the control group.

Table 1. Target gene primer sequence

| Genes | Forward Sequence | Reverse Sequence | Pathways |
|---|---|---|---|
| mMMP3 | CTCTGGAACCTGAGACATCACC | AGGAGTCCTGAGAGATTTGCGC | |
| mMMP8 | GATGCTACTACCACACTCCGTG | TAAGCAGCCTGAAGACCGTTGG | |
| mMMP12 | CACACTTCCCAGGAATCAAGCC | TTTGGTGACACGACGGAACAGG | |
| mMMP9 | GCTGACTACGATAAGGACGGCA | TAGTGGTGCAGGCAGAGTAGGA | |
| mMMP14 | GGATGGACACAGAGAACTTCGTG | CGAGAGGTAGTTCTGGGTTGAG | |
| mMMP11 | GATTGATGCTGCCTTCCAGGATG | CAGCGGAAAGTATTGGCAGGCT | Extracellular |
| mCOL15a1 | ACACCCACAGTGACTCCCAAGA | TCCTCATTGCCCACGATGTCTC | matrix |
| mCOL8a2 | GAGTGTCCTCTGGCGGCGGA | AGTCCATTGGCAGCATCGGTAG | |
| mTGFb2 | TTGTTGCCCTCCTACAGACTGG | GTAAAGAGGGCGAAGGCAGCAA | |
| mTGFb3 | AAGCAGCGCTACATAGGTGGCA | GGCTGAAAGGTGTGACATGGAC | |
| mITGA6 | CATCACGGCTTCTGTGGAGATC | CATTGTCGTCTCCACATCCTTCC | |
| mLAMB3 | TGACCAGACCTATGGACACGTG | GTCACAGTGACCTCGTTGGCAT | |
| mLOXL1 | CGACTATGACCTCCGAGTGCTA | GTAGTGGCTGAACTCGTCCATG | |
| mCCL4 | ACCCTCCCACTTCCTGCTGTTT | CTGTCTGCCTCTTTTGGTCAGG | |
| mS100a9 | TGGTGGAAGCACAGTTGGCAAC | CAGCATCATACACTCCTCAAAGC | |
| mCD68 | GGCGGTGGAATACAATGTGTCC | AGCAGGTCAAGGTGAACAGCTG | |
| mCSF1 | GCCTCCTGTTCTACAAGTGGAAG | ACTGGCAGTTCCACCTGTCTGT | |
| mFCGR1 | ACCTGAGTCACAGCGGCATCTA | TGACACGGATGCTCTCAGCACT | |
| mADAM8 | TGCCAACGTGACACTGGAGAAC | GCAGACACCTTAGCCAGTCCAA | |
| mS100a8 | CAAGGAAATCACCATGCCCTCTA | ACCATCGCAAGGAACTCCTCGA | Inflammatory |
| mSAA1 | GGAGTCTGGGCTGCTGAGAAAA | TGTCTGTTGGCTTCCTGGTCAG | response |
| mCCL2 | GCTACAAGAGGATCACCAGCAG | GTCTGGACCCATTCCTTCTTGG | |
| mCD14 | TTGAACCTCCGCAACGTGTCGT | CGCAGGAAAAGTTGAGCGAGTG | |
| mICAM1 | AAACCAGACCCTGGAACTGCAC | GCCTGGCATTTCAGAGTCTGCT | |
| mTNIP2 | AACCAGGAGCTGACAGCCATGA | CCAGCTCTTGAATCCTACTGTGC | |
| mITGAM | TACTTCGGGCAGTCTCTGAGTG | ATGGTTGCCTCCAGTCTCAGCA | |
| mCCL19 | TCGTGAAAGCCTTCCGCTACCT | CAGTCTTCGGATGATGCGATCC | |
| mGAPDH | GTCTCCTCTGACTTCAACAGCG | ACCACCCTGTTGCTGTAGCCAA | Housekeeping |

*Statistics Analysis*

Experiments were conducted in triplicate. All data are expressed as the mean ± standard deviation (SD). Statistical significance was analyzed by *t*-test using GraphPad Prism software 9 (GraphPad Software Inc., San Diego, CA, USA). All *p*-values reported are two-sided, and significance was set at $p < 0.05$. * *p*-values < 0.05, ** *p*-values < 0.01, *** *p*-values < 0.001, and **** *p*-values < 0.0001.

# Results

*Isolation, Expansion, and Characterization of NK Cells*

Repetitive inoculation of NK cells for the treatment of liver cirrhosis, an irreversible chronic liver disease, was conducted. For this experiment, the sufficient number of NK cells was obtained by carrying out negative selection of NK cells from mouse splenocytes and expanding them in an appropriate medium containing cytokines for 7 days (Figure 1).

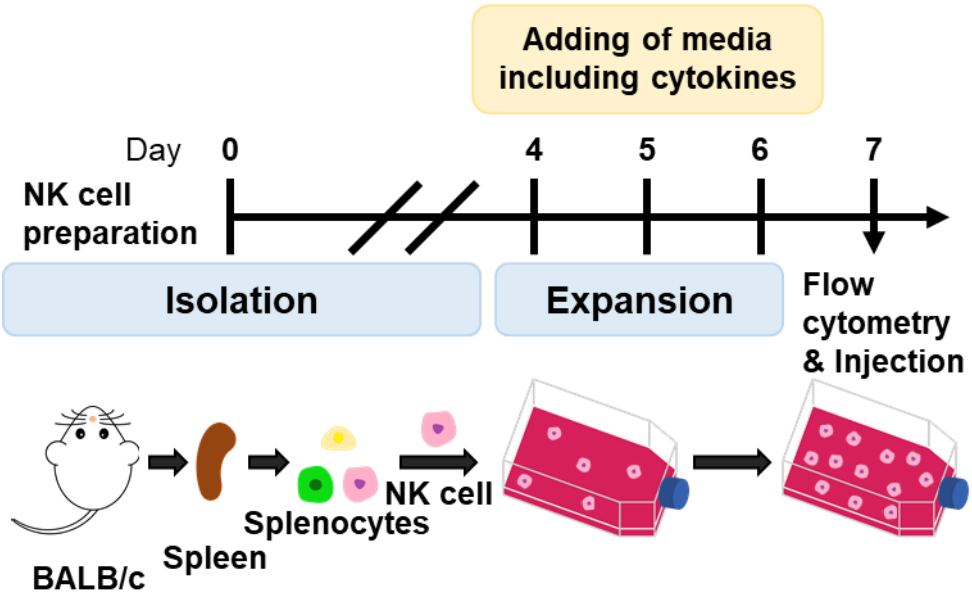


Figure 1. Schematic time course of natural killer (NK) cell isolation and expansion

Mouse spleen were crushed to obtain the splenocytes. Then, only NK cells are isolated by magnetic-activated cell sorting (MACS) method, and then cultured in NK cell-specific medium to expand NK cells.

The identity and purity of the isolated NK cells were verified using flow cytometry, and the expanded cell population was sorted and analyzed using the NK cell-specific marker NKp46. CD3e-NKp46+ NK cells, CD3e+ or CD19+ cells, and NKp46+NKG2D+ NK cells were >98%, <2%, and 61.55 ± 3.47%, respectively, in the expanded population, indicating the purity of the NK cells (Figure 2). The number of NK cells increased by approximately 13.55 ± 2.40-fold on day 7 compared to day 0 (Figure 3A), without any significant difference in cell viability (97.18 ± 4.46% and 94.92 ± 1.98% on day 0 and day 7, respectively) (Figure 3B). Finally, we identified significantly higher levels of IFN-$\gamma$ secretion in the day 7 cells compared to in the day 1 cells (Figure 3C).

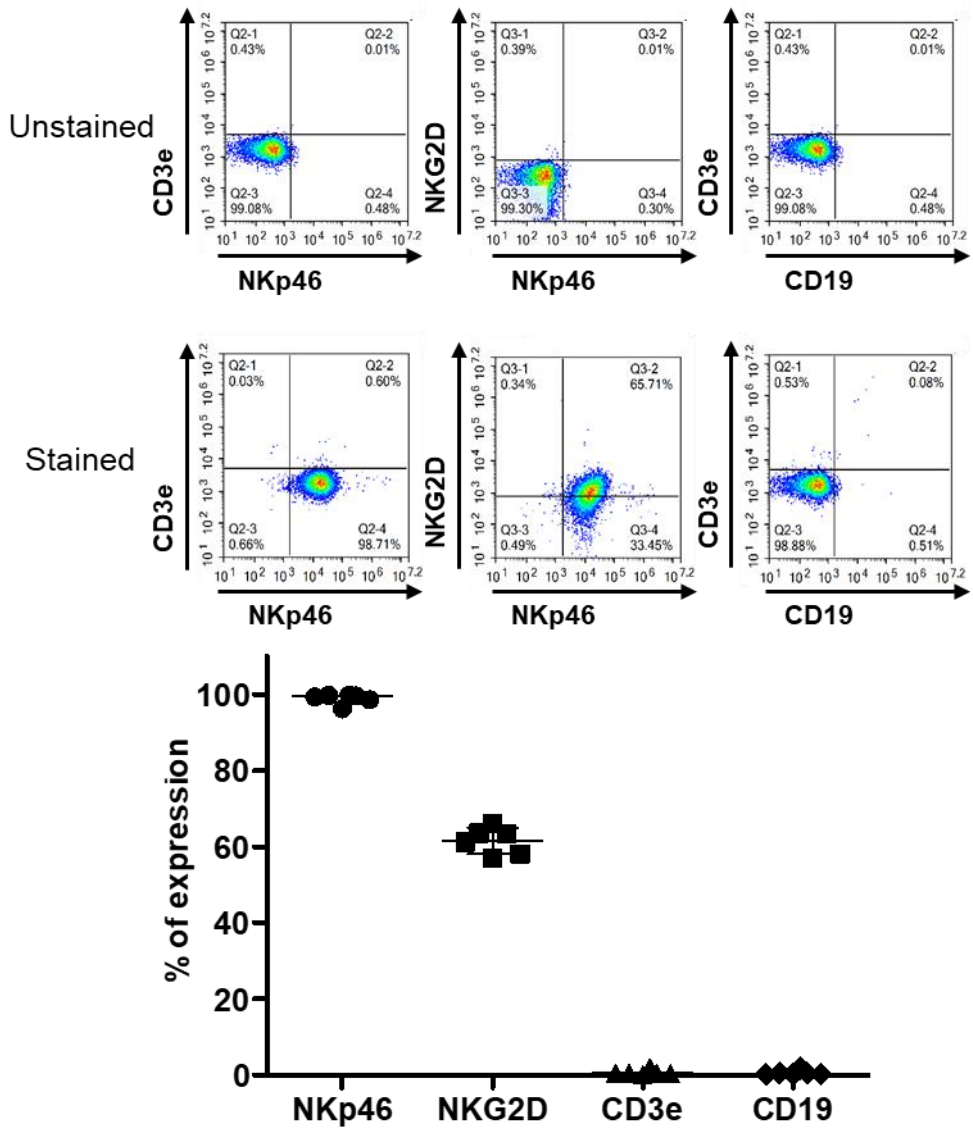


Figure 2. Flow cytometric analysis of the isolated and expanded NK cell population

Expanded NK cells were analyzed by flow cytometry. Analysis was performed using NK-specific marker NKp46, its activation marker NKG2D, T cell marker CD3e, and B cell marker CD19. CD3e-

NKp46+ NK cells, CD3e+ or CD19+ cells, and NKp46+NKG2D+ NK cells were >98%, <2%, and 61.55 ± 3.47%, respectively, in the expanded population. NKp46, natural killer cell p46-related protein. NKG2D, natural killer group 2, member D. CD3e, cluster of differentiation 3 epsilon. CD19, cluster of differentiation 19.

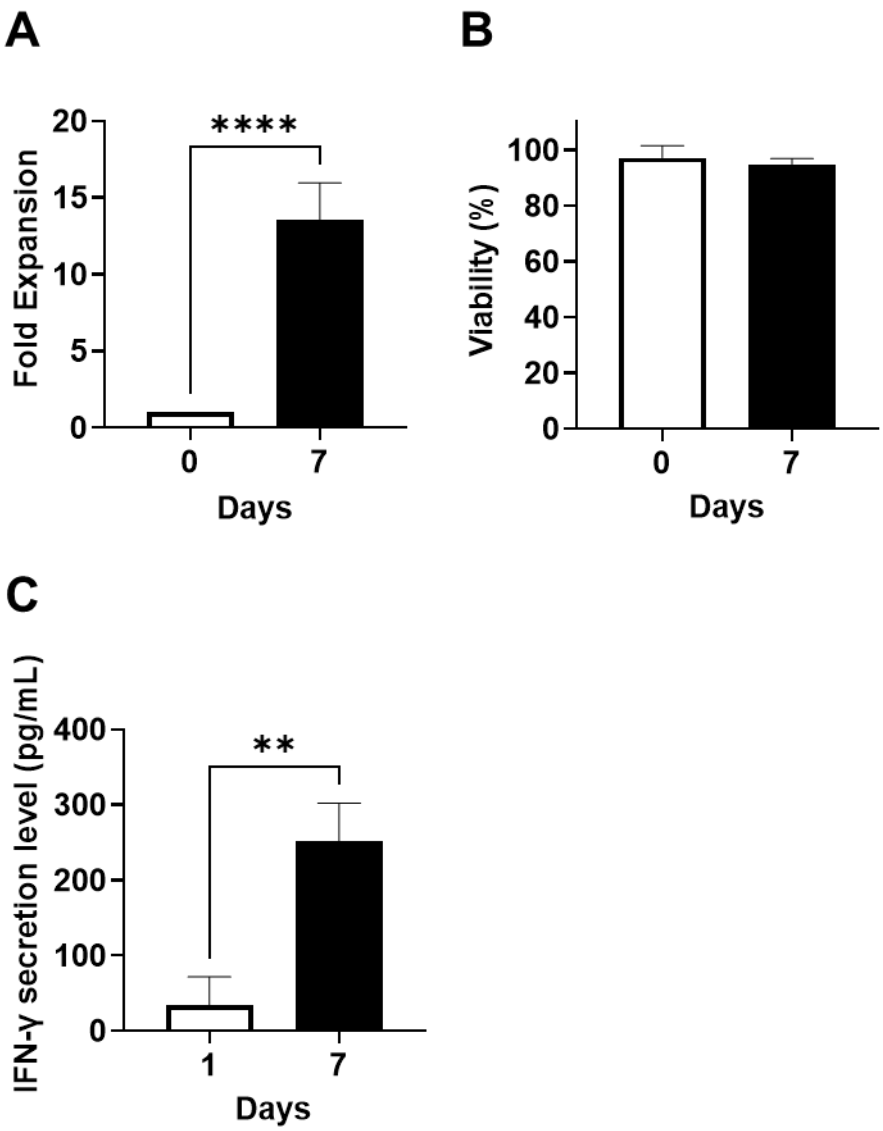


Figure 3. Validation of the expanded NK cell population

Comparison before and after 7 days of expansion. A. Cell number. B. Cell viability. C. IFN−γ secretion level.

*Significant Decrease in Collagen Deposition after Repetitive NK Cell Inoculation in the $CCl_4$-Induced Liver Cirrhosis Mouse Model*

To evaluate the effectiveness of NK cell therapy, liver tissues were analyzed 3 weeks after the initial intraperitoneal injection of $CCl_4$ to induce liver cirrhosis. Mice were injected with $CCl_4$ twice a week for 3 weeks (Figure 4A), and liver tissues were harvested 3 weeks after the first $CCl_4$ injection to verify cirrhosis. The tissue specimens were stained for H&E (Figure 4B) and Sirius red-based collagen levels (Figure 4C), showing that the liver specimens from the mineral-oil-treated control group were intact, whereas those of the $CCl_4$-treated group had high collagen deposition with liver fibrotic lesions. Based on these results, the $CCl_4$-treated mice could be used for further *in vivo* studies.

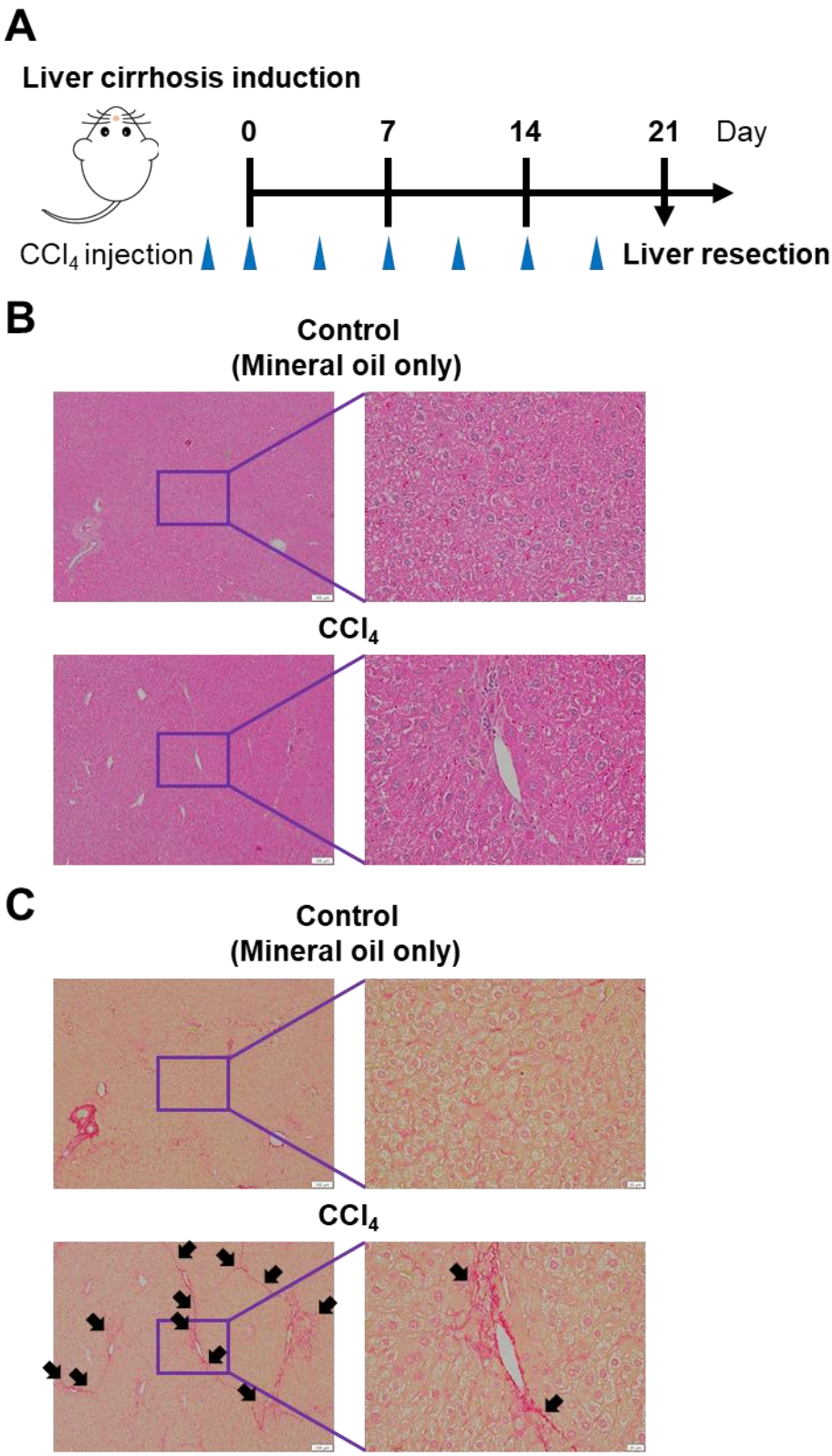
A
Liver cirrhosis induction
0
7
14
21
Day
CCl4 injection
Liver resection
B
Control
(Mineral oil only)
CCl4
C
Control
(Mineral oil only)
CCl4

**Figure 4. Evaluation of the $CCl_4$-induced liver cirrhosis mouse model**

A. Schematic time course of the $CCl_4$-induced liver cirrhosis mouse model. B. Representative images of H&E staining in the control (mineral oil only) and $CCl_4$-induced liver cirrhosis mouse model. C. Representative images of Sirius red staining in the control (mineral oil only) and $CCl_4$-induced liver cirrhosis mouse model. The image on the right was obtained from the left purple square area. Black arrow, pathological positive staining of fibrosis. Magnification. Left, 40X, Right, 200X.

To verify the efficacy of the NK cell therapy, the NK cells were injected intravenously once a week from 3 weeks after the first $CCl_4$ injection into $CCl_4$-induced liver cirrhosis mice (Figure 5A). After a total of six injections of NK cells ($1 \times 10^6$ cells each), liver tissues were harvested, and Sirius red staining was performed. The repetitive NK cell inoculations resulted in a significant reduction in the fibrotic area in the liver sections (Figure 5B). The liver tissues from the $CCl_4$-only treatment group exhibited more fibrotic areas compared to those from the $CCl_4$ + NK cell treatment group. Quantitative analysis of the fibrotic areas confirmed that the $CCl_4$ + NK cell treatment group had significantly less fibrosis compared to the $CCl_4$-only treatment group, similar to the control group (Figure 5B).

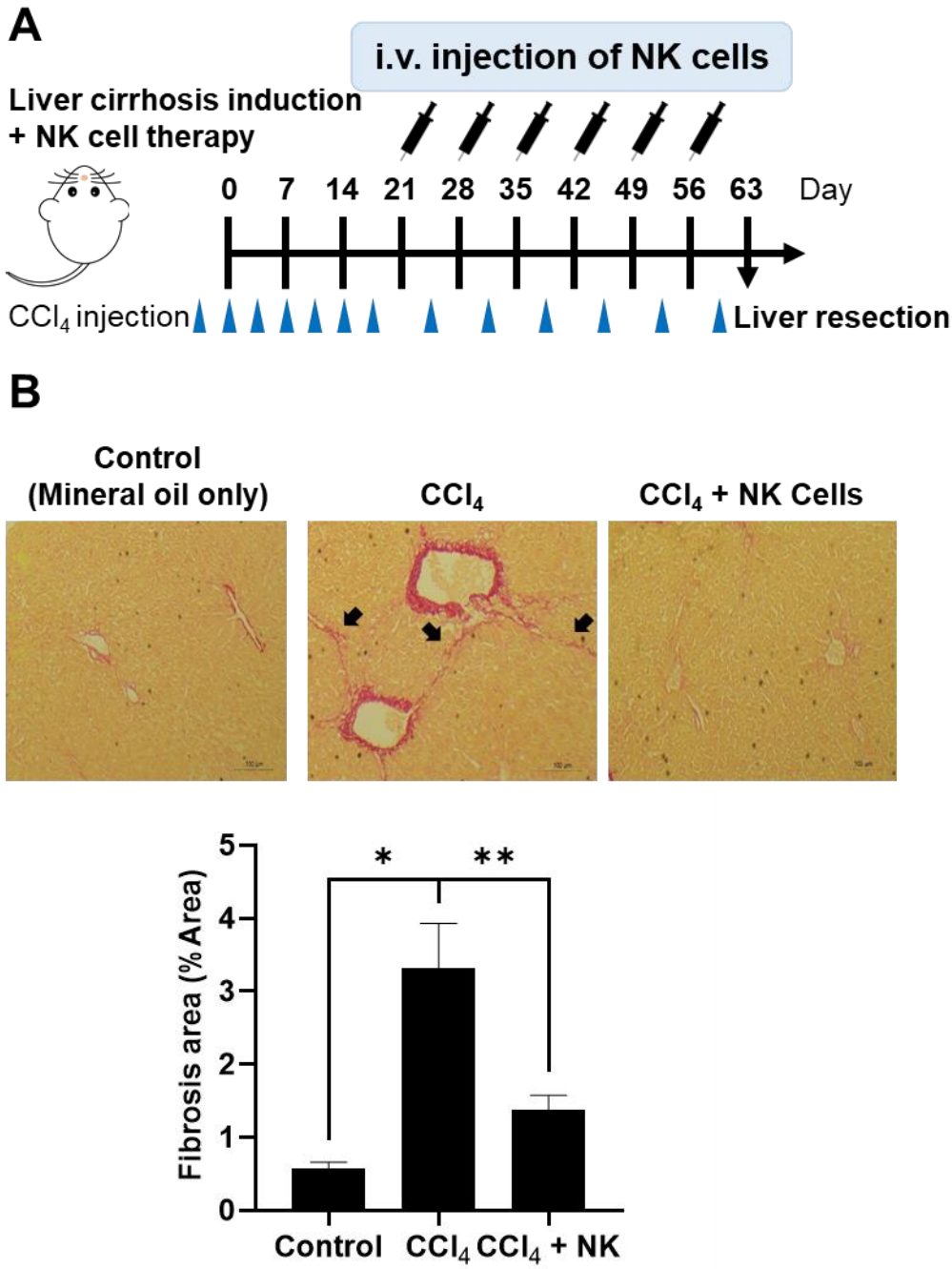


Figure 5. Reduced liver cirrhosis progression after NK cell transplantation in the $CCl_4$-induced liver cirrhosis mouse model

Representative images of Sirius red staining compared across control (mineral oil only), $CCl_4$-only treated, and $CCl_4$ + NK cell-treated groups. Scale bar, 200 $\mu$m. Black arrow, pathological positive staining of fibrosis. Right graph demonstrates the quantitative analysis of the red fibrotic area. Data represent means $\pm$ SD. * p-values < 0.05.

*Suppression of Fibrosis after NK Cell Therapy*

Further investigation was conducted to explore the potential mechanism of cirrhosis suppression by NK cell therapy. Immunofluorescence analysis was performed to assess the association of NK cell therapy with activated hepatic stellate cells and macrophages in the liver. The level of TGF-$\beta$1 secreted from the activated macrophages in the liver was higher in the $CCl_4$-only treatment group than in the normal liver (Figure 6A, D). Alpha-smooth muscle actin ($\alpha$-SMA) levels, known to be activated in HSCs, and F4/80, a macrophage infiltration marker, were increased in the $CCl_4$-only treatment group (Figure 6B, C, D). In contrast, significant reductions of TGF-$\beta$1 (Figure 6A, D), activated HSCs (Figure 6B, D), and macrophage infiltration (Figure 6C, D) were observed in the $CCl_4$ + NK cell treatment group. These results suggested that NK cell therapy could reduce fibrosis by decreasing inflammation in the liver.

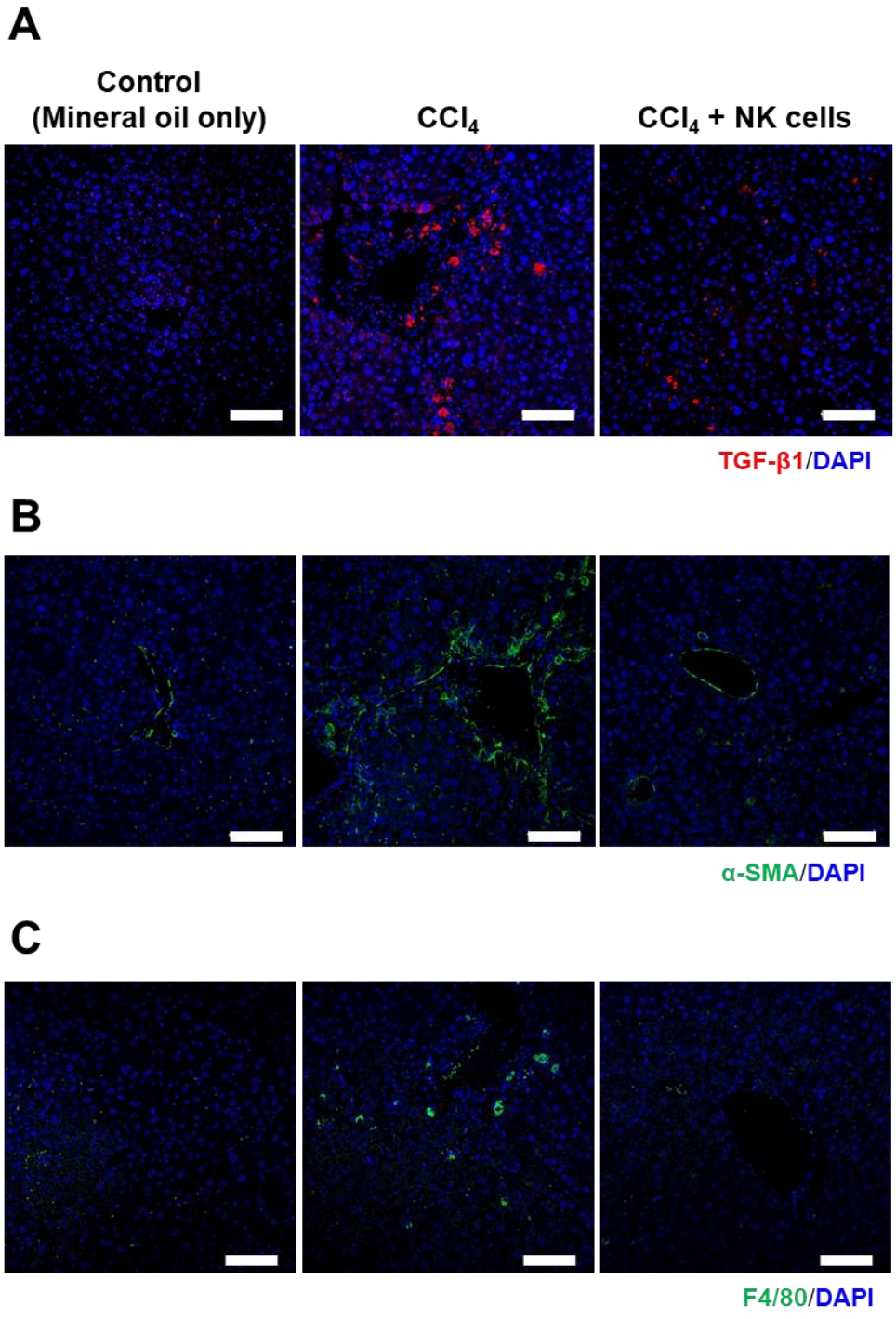
A
Control
(Mineral oil only)
CCl4
CCl4 + NK cells
TGF-β1/DAPI
B
α-SMA/DAPI
C
F4/80/DAPI

**D**

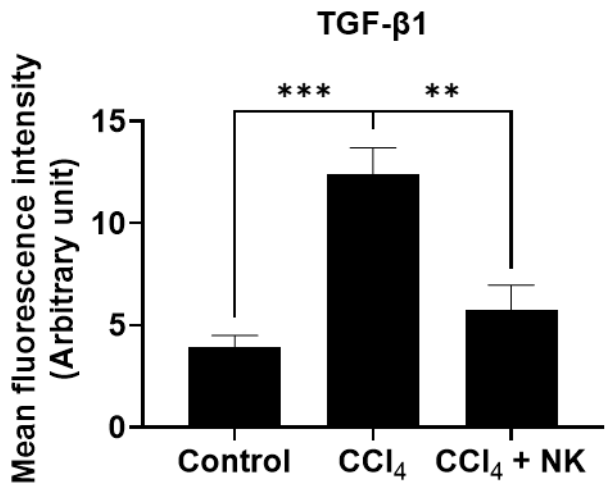
TGF-β1
Mean fluorescence intensity (Arbitrary unit)
***
**
15
10
5
0
Control
CCl4
CCl4 + NK

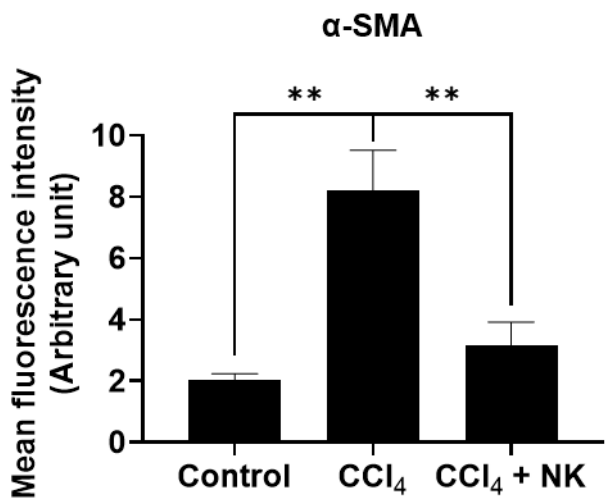
α-SMA
Mean fluorescence intensity (Arbitrary unit)
**
**
10
8
6
4
2
0
Control
CCl4
CCl4 + NK

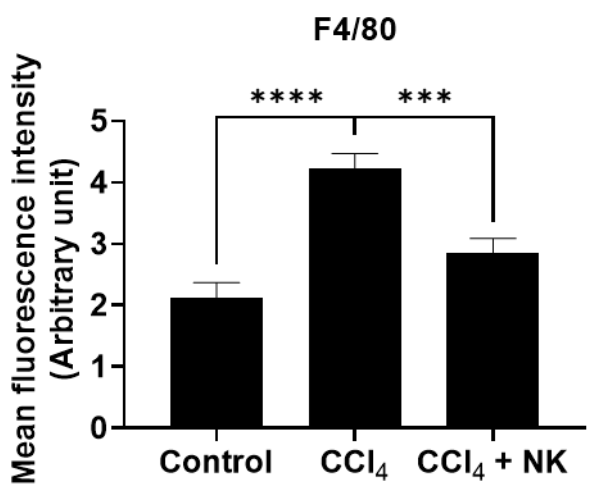
F4/80
Mean fluorescence intensity (Arbitrary unit)
****
***
5
4
3
2
1
0
Control
CCl4
CCl4 + NK

**Figure 6. Decrease in fibrosis after NK cell transplantation in the $CCl_4$-induced liver cirrhosis mouse model**

A. Representative TGF-$\beta$1 (pro-fibrogenic and inflammatory marker) immunofluorescence images. B. Representative $\alpha$-SMA (hepatic stellate activation marker) immunofluorescence images. C. Representative F4/80 (macrophage surface marker) immunofluorescence images. D. Quantitative analysis of immunofluorescence images. Scale bar, 100 $\mu$m. Data represent means ± SD. * p-values < 0.05, ** p-values < 0.01, *** p-values < 0.001, and **** p-values < 0.0001.

*Optical Image-Based In Vivo Tracking of NK Cells Derived from Codon-Optimized Luciferase-Expressing Transgenic Mice in the $CCl_4$-Induced Liver Cirrhosis Mouse Model*

To track the inoculated NK cells, BLI was used, as tracing the inoculated NK cells may be important to elucidate their site-specific roles. However, very low infection efficacy of NK cells using luciferase lentivirus is typically seen due to the intrinsic resistance of NK cells to external virus infection. Thus, we used transgenic mice stably expressing the codon-optimized luciferase (luc) gene in all tissues to obtain the NK-luc cells. After harvesting the spleens of the codon-optimized luciferase transgenic mice, NK-luc cells were isolated and expanded for 7 days (Figure 7).

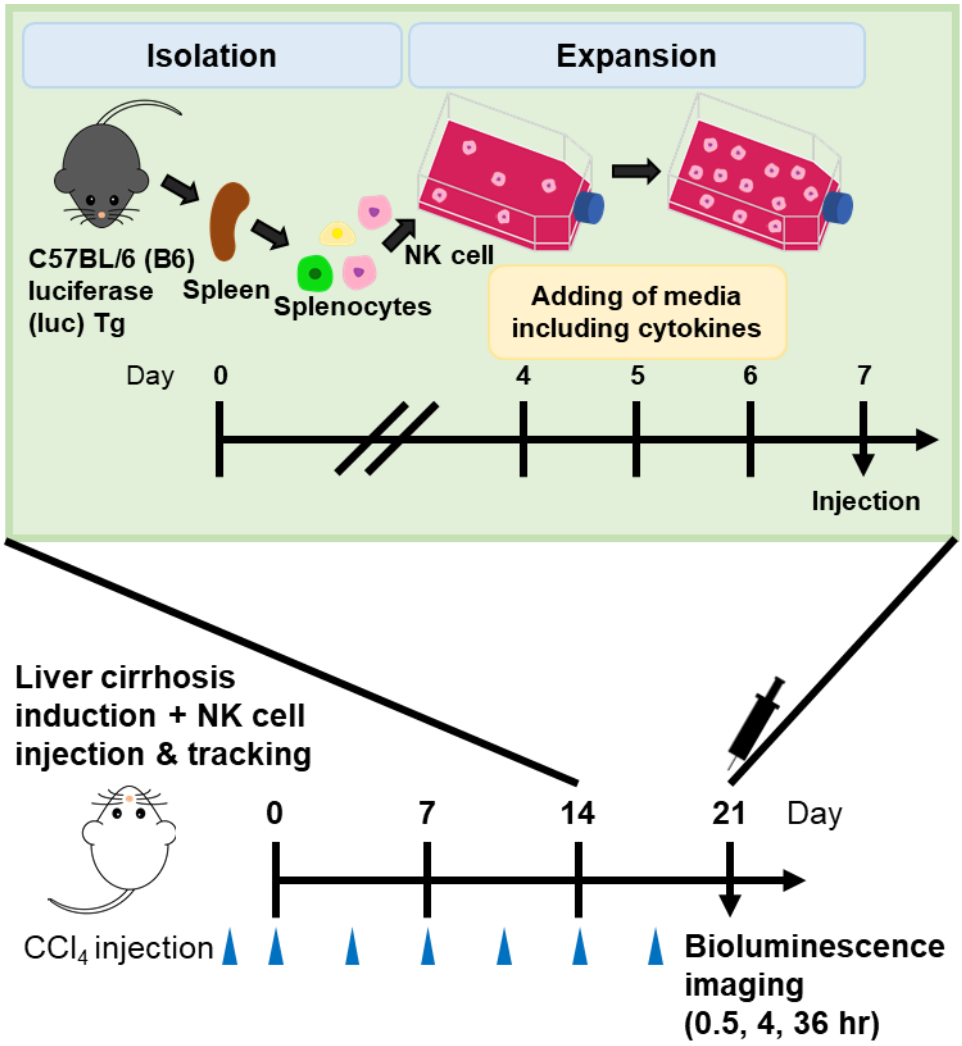


Figure 7. Schematic time course of $CCl_4$ treatment and bioluminescence imaging (BLI) for NK cell tracking

The cell number-dependent luminescence signal was evaluated in splenocytes from the codon-optimized luciferase transgenic mice and isolated NK and NK-luc cells using an *in vitro* luminescence assay (Figure 8A, B). NK-luc cells, showing a higher luminescence signal than normal NK cells (Figure 8B), were injected intravenously into the mice (Figure 9A, B). BLI results showed that the inoculated NK-luc cells remained in the liver in the $CCl_4$ + NK-luc cell treatment group compared with the control + NK-luc cell treatment group (Figure 9A, B). When organs were harvested after imaging at 36 hours, the livers of the $CCl_4$ + NK-luc cell treatment group showed a higher luminescence signal than those of the control + NK-luc cell treatment group. The bioluminescence signals in the other organs, with the exception of the lungs, were low in both groups. These results illustrated that the inoculated NK cells resided in the cirrhotic liver and were involved in reducing the progression of cirrhosis.

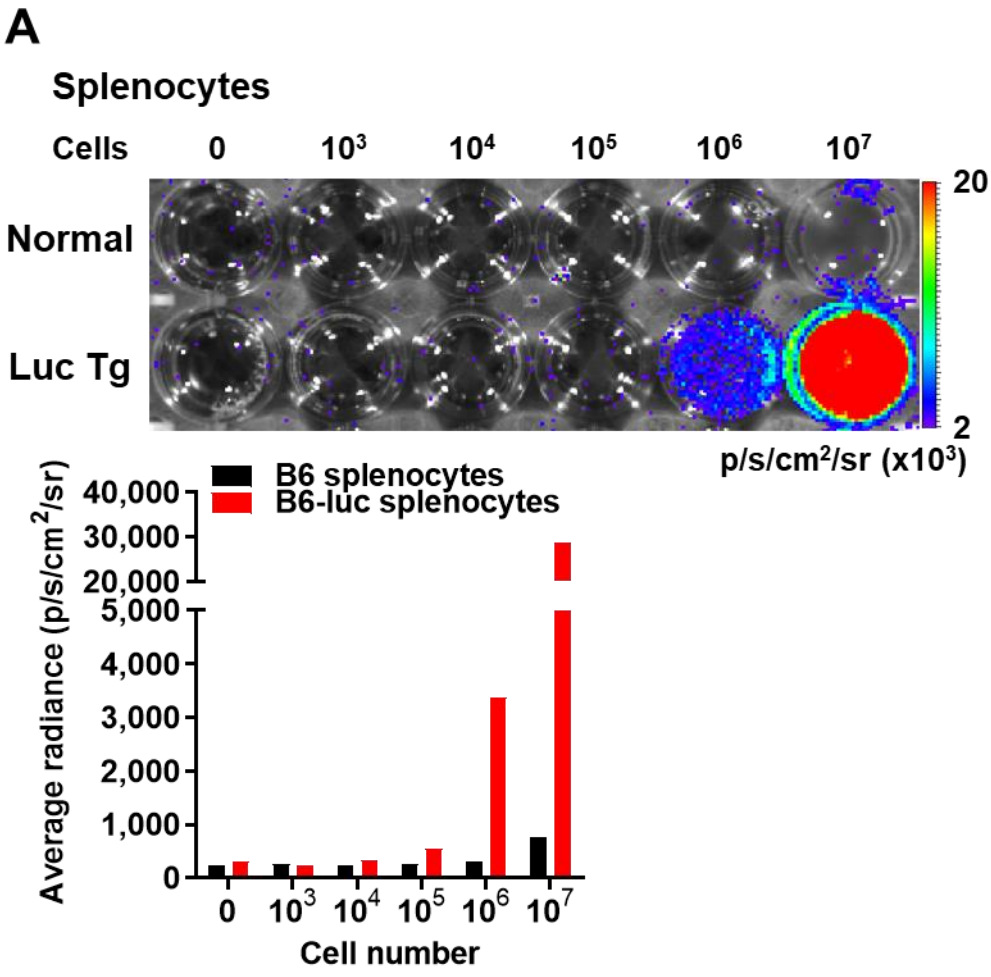
A
Splenocytes
Cells
0
10^3
10^4
10^5
10^6
10^7
Normal
Luc Tg
20
2
p/s/cm²/sr (x10³)
B6 splenocytes
B6-luc splenocytes
Average radiance (p/s/cm²/sr)
40,000
30,000
20,000
5,000
4,000
3,000
2,000
1,000
0
Cell number
B
NK cells
NK-luc cells
Bioluminescence intensity (Arbitrary unit)
200,000
150,000
100,000
20,000
15,000
10,000
5,000
0
10^1
10^2
Cell number

Figure 8. *In vitro* bioluminescence assay of splenocytes and expanded NK cells from codon-optimized luciferase transgenic mice

A. Representative bioluminescence image and quantitative analysis of splenocytes from normal mouse and luciferase transgenic mouse.

B. *In vitro* bioluminescence assay of NK and NK-luc cells.

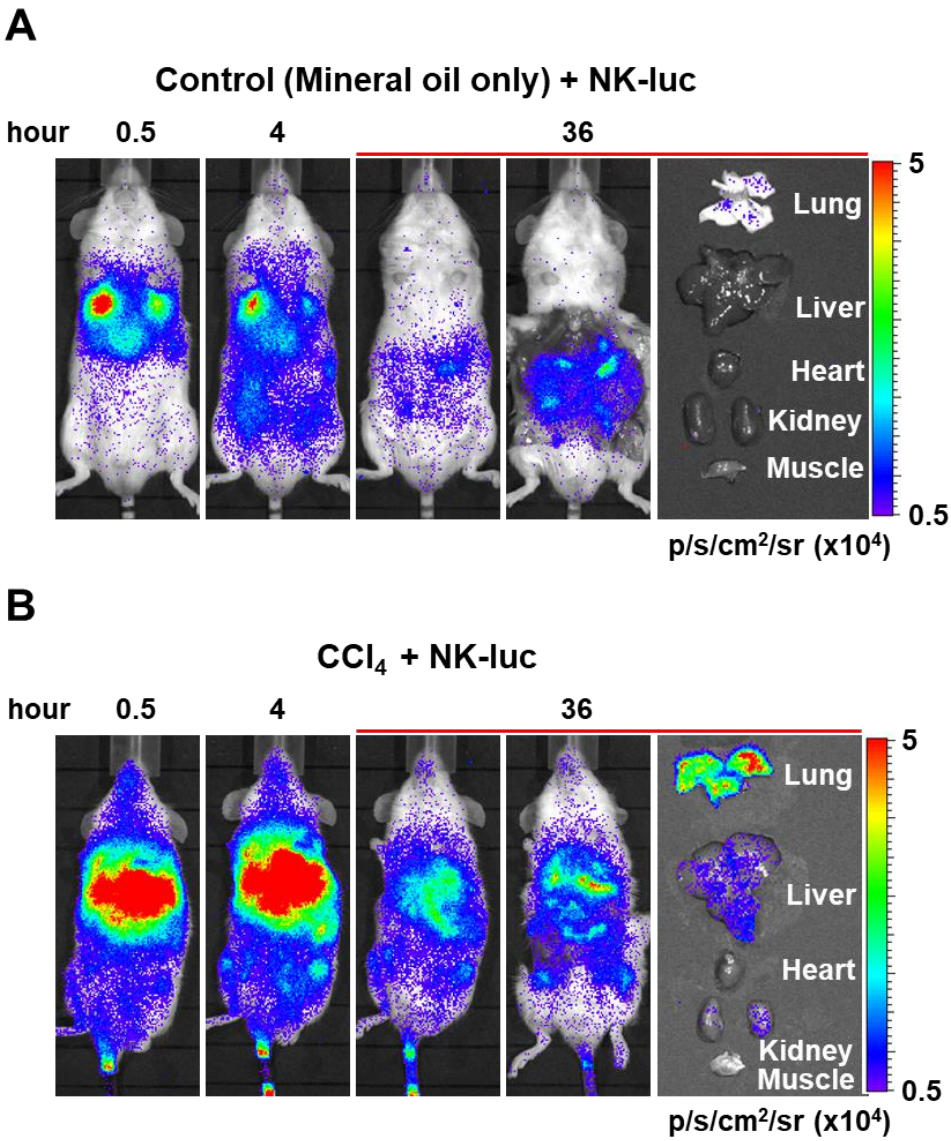


Figure 9. *In vivo* bioluminescence tracking of NK cells in the $CCl_4$-induced liver cirrhosis mouse model

Representative bioluminescence imaging (BLI). A. Control (Mineral oil only) + NK-luc cell. B. $CCl_4$ + NK-luc cell. After imaging at 36 hours, mice were sacrificed, and organs were harvested (Control

(Mineral oil only) + NK-luc group (n = 2), $CCl_4$ + NK-luc group (n = 3)).

*Gene Expression Profiling of Liver Cirrhosis Mouse Model after NK Cell Therapy*

To gain insights into the therapeutic mechanisms underlying NK cell therapy, gene expression profiling was conducted using QuantSeq 3′ mRNA sequencing. Conventional RNA sequencing was conducted to examine the gene expression profile of the NK cell-treated liver cirrhosis mouse model. QuantSeq 3′ mRNA sequencing was performed on the saline, $CCl_4$, and $CCl_4$ + NK cell-treated ($CCl_4$ + NK) groups. Figure 10A shows significantly up- or down-regulated gene expression profiles, as determined by cluster heatmap analysis. DEGs were identified as genes up- or down-regulated with a ± 1.5-fold change (log2 = 1). As summarized in the expression plots, we identified 295 and 1034 of up- and down-regulated DEGs in the $CCl_4$ compared with the saline group and 319 and 176 of up- and down-regulated DEGs in $CCl_4$ + NK cell-treated group compared with the $CCl_4$ group (Figure 10B).

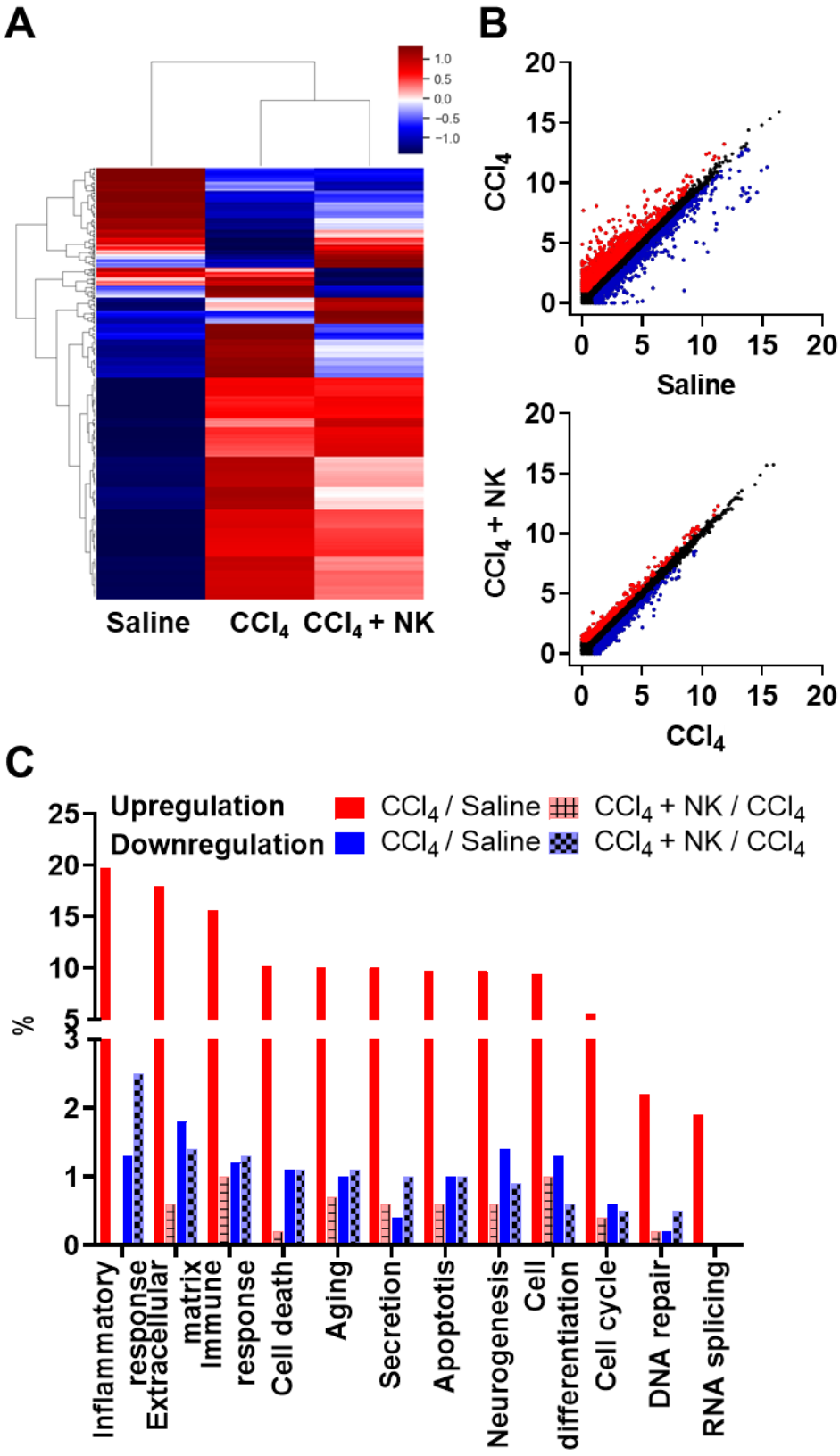
A
1.0
0.5
0.0
−0.5
−1.0
Saline
CCl4
CCl4 + NK
B
CCl4
Saline
CCl4 + NK
CCl4
C
Upregulation
Downregulation
CCl4 / Saline
CCl4 + NK / CCl4
CCl4 / Saline
CCl4 + NK / CCl4
%
Inflammatory response
Extracellular matrix
Immune response
Cell death
Aging
Secretion
Apoptotis
Neurogenesis
Cell differentiation
Cell cycle
DNA repair
RNA splicing

**Figure 10. QuantSeq analysis of treatment-dependent differentially expressed genes (DEGs)**

A. Cluster heatmap of 1532 gene sets (fold-change = 1.5, p-value = 0.050, normalized data (log2 = 1)). The relative gene expression level was indicated by red for high expression and blue for low expression. B. Scatter plot of DEGs. C. Bar graph of gene ontology (GO). The bar indicates the GO terms related to gene functions and the percentage of differential expression in upregulated or downregulated genes in each category. Red and blue indicate >1.5-fold increased and decreased expression, respectively.

The gene ontology (GO)−based bioinformatics analysis of the DEGs of the $CCl_4$/saline and $CCl_4$ + NK/$CCl_4$ groups is presented in Figure 10C. The upregulation of the inflammatory response (19.7%)− and extracellular matrix (ECM) (17.9%)−related genes was the highest in the $CCl_4$/saline group. The upregulation of the inflammatory response and ECM genes decreased after NK cell treatment. In addition, inflammatory response (2.5%)− and ECM (1.4%)−related genes were downregulated in the $CCl_4$ + NK/$CCl_4$ group. Since inflammatory response and ECM play an important role in cirrhosis, we examined these two categories of genes in the DEGs. In 1532 DEGs, 33 downregulated genes in the ECM (Table 2) and 41 downregulated genes in the inflammatory response (Table 3) were found.

Table 2. Expression levels of DEGs involved in the extracellular matrix. The expression level of each gene is reported as the read count normalized to the log2 value. Red and blue background colors were used to visualize increased and decreased gene expressions, respectively, with the intensity of color representing the magnitude of change for fold-change values.

Genes involved in the extracellular matrix

| Gene symbol | Fold change | | Normalized data (log2) | | |
|---|---|---|---|---|---|
| | $CCl_4$ / Saline | $CCl_4$ + NK / $CCl_4$ | Saline | $CCl_4$ | $CCl_4$ + NK |
| SERPINE1 | 12.519 | 0.139 | 1.378 | 5.024 | 2.178 |
| THBS4 | 4.682 | 0.370 | 0.000 | 2.227 | 0.792 |
| THBS1 | 3.378 | 0.373 | 1.079 | 2.835 | 1.413 |
| CRISPLD2 | 5.071 | 0.459 | 1.299 | 3.641 | 2.516 |
| MMP3 | 1.603 | 0.466 | 0.762 | 1.443 | 0.340 |
| MMP12 | 15.310 | 0.494 | 0.638 | 4.575 | 3.557 |
| ELAN | 2.534 | 0.500 | 0.000 | 1.341 | 0.340 |
| LTBP2 | 8.797 | 0.505 | 0.188 | 3.325 | 2.338 |
| MMP8 | 2.836 | 0.505 | 0.430 | 1.935 | 0.949 |
| BMPER | 3.474 | 0.512 | 0.430 | 2.227 | 1.261 |
| LOXL1 | 5.101 | 0.516 | 1.339 | 3.690 | 2.734 |
| PLXDC2 | 5.697 | 0.516 | 0.875 | 3.385 | 2.430 |
| COL15a1 | 2.356 | 0.524 | 2.501 | 3.737 | 2.804 |
| OLFML2B | 1.865 | 0.528 | 0.638 | 1.537 | 0.615 |
| ANGPTL7 | 1.977 | 0.556 | 1.126 | 2.109 | 1.261 |
| ADAMTS1 | 3.073 | 0.559 | 2.603 | 4.223 | 3.384 |
| TGFb2 | 3.607 | 0.573 | 0.503 | 2.354 | 1.550 |
| LRRC24 | 2.390 | 0.58 | 1.079 | 2.336 | 1.550 |
| MGP | 6.283 | 0.582 | 2.620 | 5.271 | 4.491 |
| ITGA6 | 2.989 | 0.582 | 1.126 | 2.705 | 1.923 |

| | | | | | |
|---|---|---|---|---|---|
| MFAP5 | 1.695 | 0.585 | 0.354 | 1.115 | 0.34 |
| LABM3 | 2.051 | 0.588 | 1.031 | 2.067 | 1.300 |
| VASN | 1.718 | 0.59 | 3.625 | 4.405 | 3.644 |
| TGFb3 | 2.952 | 0.596 | 1.031 | 2.593 | 1.845 |
| MMP9 | 3.679 | 0.604 | 0.188 | 2.067 | 1.339 |
| FMOD | 3.765 | 0.611 | 0.820 | 2.732 | 2.021 |
| WNT4 | 3.284 | 0.625 | 0.638 | 2.354 | 1.676 |
| MMP14 | 2.711 | 0.627 | 5.089 | 6.527 | 5.854 |
| MMP11 | 1.719 | 0.628 | 0.981 | 1.763 | 1.091 |
| VWA1 | 1.663 | 0.646 | 0.572 | 1.306 | 0.677 |
| IL16 | 2.404 | 0.647 | 1.453 | 2.719 | 2.090 |
| LGALS3 | 23.571 | 0.651 | 1.525 | 6.084 | 5.465 |
| COL8a2 | 2.336 | 0.656 | 0.430 | 1.654 | 1.045 |

Table 3. Expression levels of DEGs involved in the inflammatory response. The expression level of each gene is reported as the read count normalized to the log2 value. Red and blue background colors were used to visualize increased and decreased gene expressions, respectively, with the intensity of color representing the magnitude of change for fold-change values.

Genes involved in the inflammatory response

| Gene symbol | Fold change | | Normalized data (log2) | | |
|---|---|---|---|---|---|
| | $CCl_4$ / Saline | $CCl_4$ + NK / $CCl_4$ | Saline | $CCl_4$ | $CCl_4$ + NK |
| SAA2 | 18.764 | 0.318 | 3.786 | 8.016 | 6.363 |
| NUPR1 | 5.942 | 0.344 | 0.188 | 2.759 | 1.220 |
| CXCL2 | 6.373 | 0.361 | 0.820 | 3.492 | 2.021 |
| THBS1 | 3.378 | 0.373 | 1.079 | 2.835 | 1.413 |
| CCL2 | 5.937 | 0.427 | 0.701 | 3.271 | 2.045 |
| SAA1 | 8.838 | 0.464 | 6.174 | 9.318 | 8.211 |
| FPR2 | 6.102 | 0.474 | 1.453 | 4.063 | 2.985 |
| CAMP | 6.952 | 0.488 | 0.000 | 2.797 | 1.763 |
| ADCYL | 1.831 | 0.488 | 0.503 | 1.376 | 0.340 |
| HPS1 | 1.708 | 0.490 | 3.191 | 3.964 | 2.935 |
| CD14 | 7.534 | 0.491 | 1.525 | 4.438 | 3.412 |
| ELANE | 2.534 | 0.500 | 0.000 | 1.341 | 0.340 |
| S100a8 | 33.124 | 0.507 | 0.981 | 6.031 | 5.050 |
| GGT5 | 1.631 | 0.540 | 1.031 | 1.736 | 0.846 |
| RELB | 6.453 | 0.541 | 0.762 | 3.452 | 2.566 |
| CXCL5 | 3.516 | 0.549 | 0.000 | 1.814 | 0.949 |
| CCL21A | 1.967 | 0.550 | 1.809 | 2.785 | 1.923 |
| CSF1 | 2.565 | 0.559 | 2.351 | 3.710 | 2.871 |
| CD68 | 5.757 | 0.560 | 2.446 | 4.972 | 4.134 |
| PPARG | 1.694 | 0.563 | 3.180 | 3.941 | 3.112 |

| | | | | | |
|---|---|---|---|---|---|
| AIM2 | 2.621 | 0.566 | 0.981 | 2.371 | 1.550 |
| CCRL2 | 4.28 | 0.566 | 0.273 | 2.371 | 1.550 |
| HCK | 6.707 | 0.573 | 0.762 | 3.507 | 2.705 |
| PLA2G7 | 5.618 | 0.575 | 2.409 | 4.899 | 4.101 |
| ADAM8 | 4.346 | 0.577 | 0.572 | 2.692 | 1.898 |
| TICAM2 | 1.898 | 0.583 | 0.701 | 1.626 | 0.846 |
| FCGR1 | 2.675 | 0.584 | 1.378 | 2.797 | 2.021 |
| S100a9 | 28.555 | 0.592 | 1.453 | 6.289 | 5.533 |
| CCL4 | 2.227 | 0.598 | 0.000 | 1.155 | 0.414 |
| BCL6 | 2.036 | 0.599 | 5.327 | 6.353 | 5.613 |
| SIGIRR | 2.070 | 0.602 | 2.953 | 4.003 | 3.270 |
| HDAC9 | 1.926 | 0.616 | 0.430 | 1.376 | 0.677 |
| HYAL3 | 1.516 | 0.620 | 0.430 | 1.031 | 0.340 |
| SMPDL3B | 3.045 | 0.621 | 1.126 | 2.732 | 2.045 |
| CCL19 | 3.173 | 0.628 | 0.097 | 1.763 | 1.091 |
| MYO9A | 6.399 | 0.635 | 0.638 | 3.316 | 2.660 |
| ORM3 | 5.913 | 0.650 | 2.311 | 4.875 | 4.255 |
| CX3CL1 | 2.860 | 0.657 | 0.572 | 2.088 | 1.483 |
| ITGAM | 5.006 | 0.661 | 0.572 | 2.896 | 2.300 |
| TNIP2 | 1.921 | 0.663 | 2.185 | 3.126 | 2.533 |
| ICAM1 | 2.885 | 0.664 | 2.518 | 4.047 | 3.456 |

*qRT-PCR Verification of the Downregulated DEGs Related to ECM and Inflammatory Response*

Expression patterns of functionally identified ECM and inflammatory response genes in downgraded DEGs were confirmed by qRT-PCR. The representative expression patterns are displayed in Figure 11A, 12A. QuantSeq 3′ mRNA sequencing expressed as a heatmap shows that the expression level of specific genes was significantly decreased in the $CCl_4$ + NK group compared to the $CCl_4$ group. Mainly, matrix metalloproteinases (MMPs) related to the degradation of the matrix and collagenases and TGF-$\beta$ related to liver fibrosis formation were identified. Regulation-related (*Ccl19*, *S100a8*, *Ccl1*, etc.) and macrophage inflammatory response (*Ccl4*, *Cd68*, etc.) genes were identified among the inflammatory response genes. For verification of the identified genes, mRNA expression levels of 13 genes (*Mmp3*, *Mmp11*, *Mmp8*, *Lamb3*, *Col15a1*, *Mmp12*, *Itga6*, *Col8a2*, *Tgfb3*, *Mmp14*, *Tgfb2*, *Mmp9*, *Loxl1*) related to the ECM and 14 genes (*Csf1*, *Ccl4*, *Tnip2*, *Ccl2*, *Fcgr1*, *Cd68*, *Cd14*, *Saa1*, *Ccl19*, *Adam8*, *Icam1*, *Itgam*, *S100a8*, *S100a9*) related to the inflammatory response were analyzed using qRT-PCR (Figure 11B, 12B). The results of the qRT-PCR verification were consistent with QuantSeq 3′ mRNA sequencing. These results elucidated the therapeutic effect of NK

cell therapy in the $CCl_4$-induced liver cirrhosis mouse model at the genetic level.

A

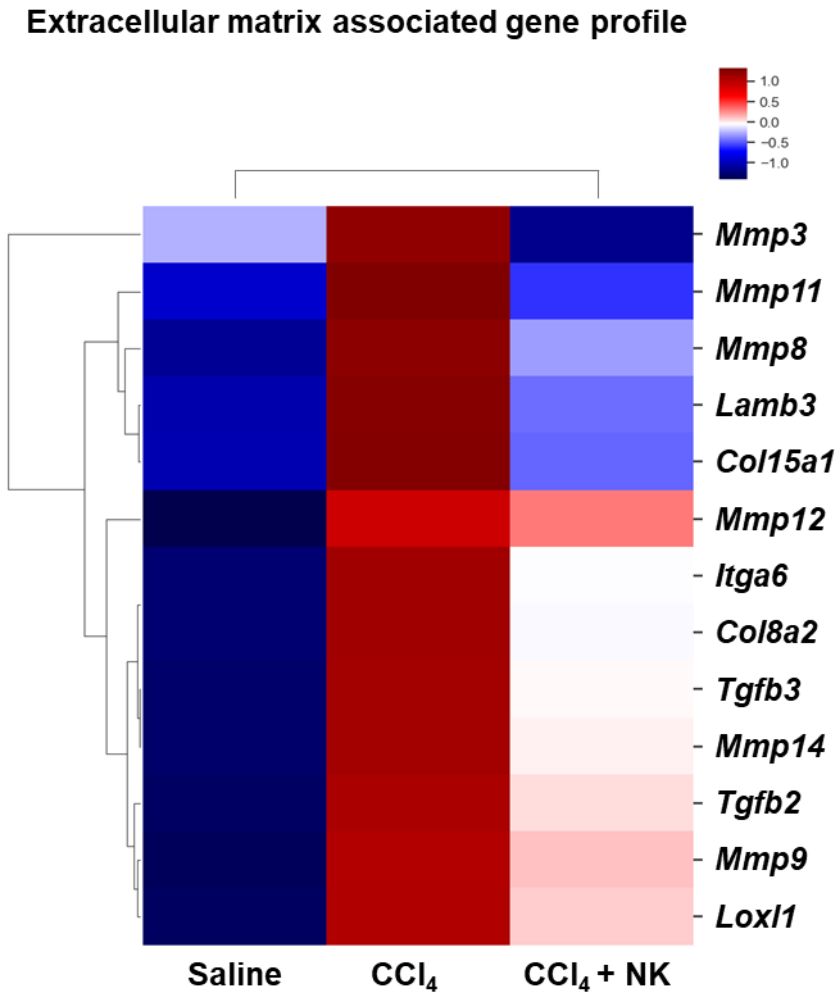
Extracellular matrix associated gene profile
1.0
0.5
0.0
−0.5
−1.0
Mmp3
Mmp11
Mmp8
Lamb3
Col15a1
Mmp12
Itga6
Col8a2
Tgfb3
Mmp14
Tgfb2
Mmp9
Loxl1
Saline
CCl4
CCl4 + NK

**B**

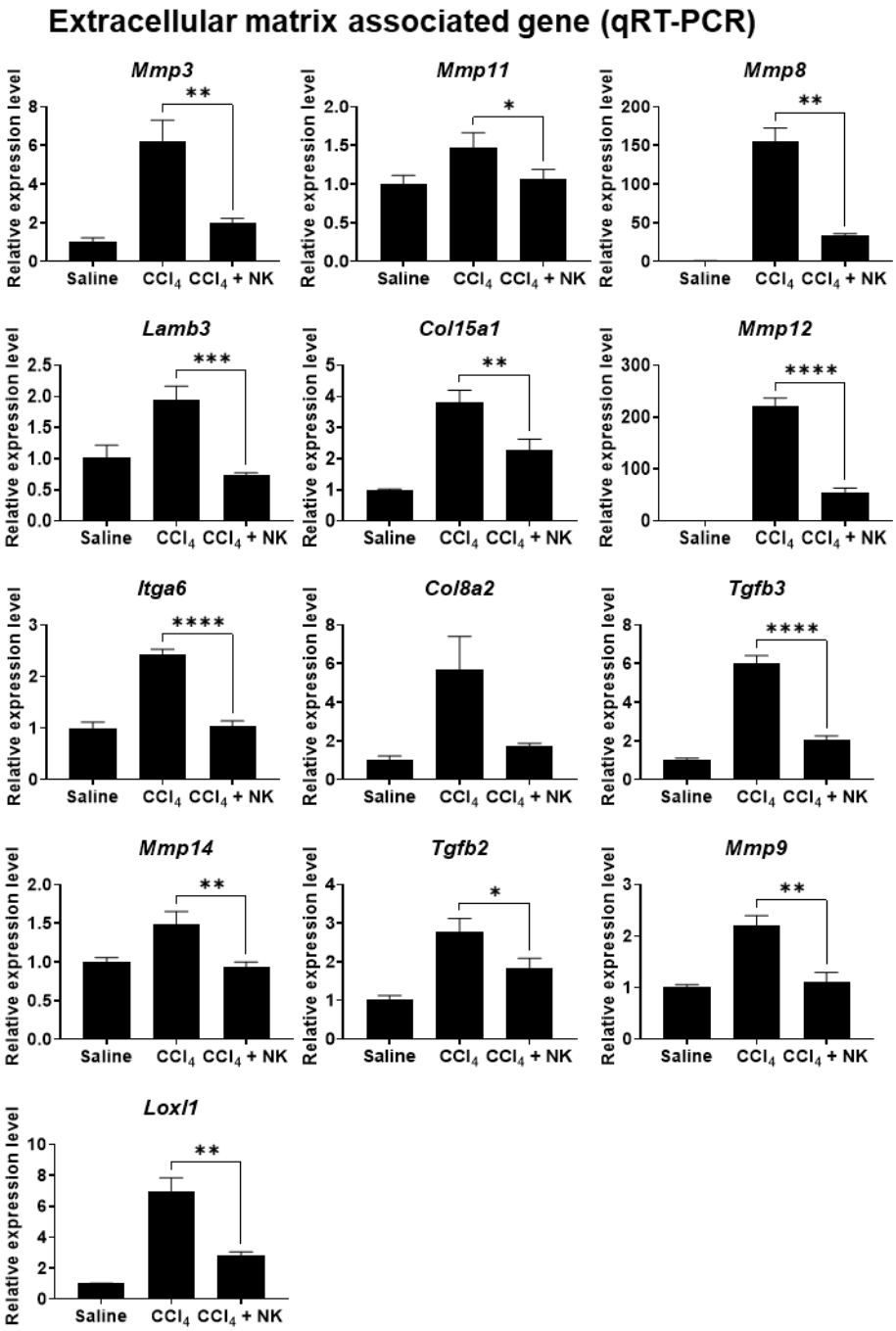
Extracellular matrix associated gene (qRT-PCR)
Mmp3
Mmp11
Mmp8
Lamb3
Col15a1
Mmp12
Itga6
Col8a2
Tgfb3
Mmp14
Tgfb2
Mmp9
Loxl1
Relative expression level
Saline
CCl4
CCl4 + NK

Figure 11. Validation of expression levels of DEGs associated with extracellular matrix by qRT-PCR

A. Cluster heatmap of upregulated extracellular matrix-associated genes (n = 13). The relative gene expression level was indicated by red for high expression and blue for low expression. B. Relative gene expression of extracellular matrix-associated genes by qRT-PCR analysis. Data are presented as mean ± SD from three independent experiments. * p-values < 0.05, ** p-values < 0.005, *** p-values < 0.001, and **** p-values < 0.0001.

**A**

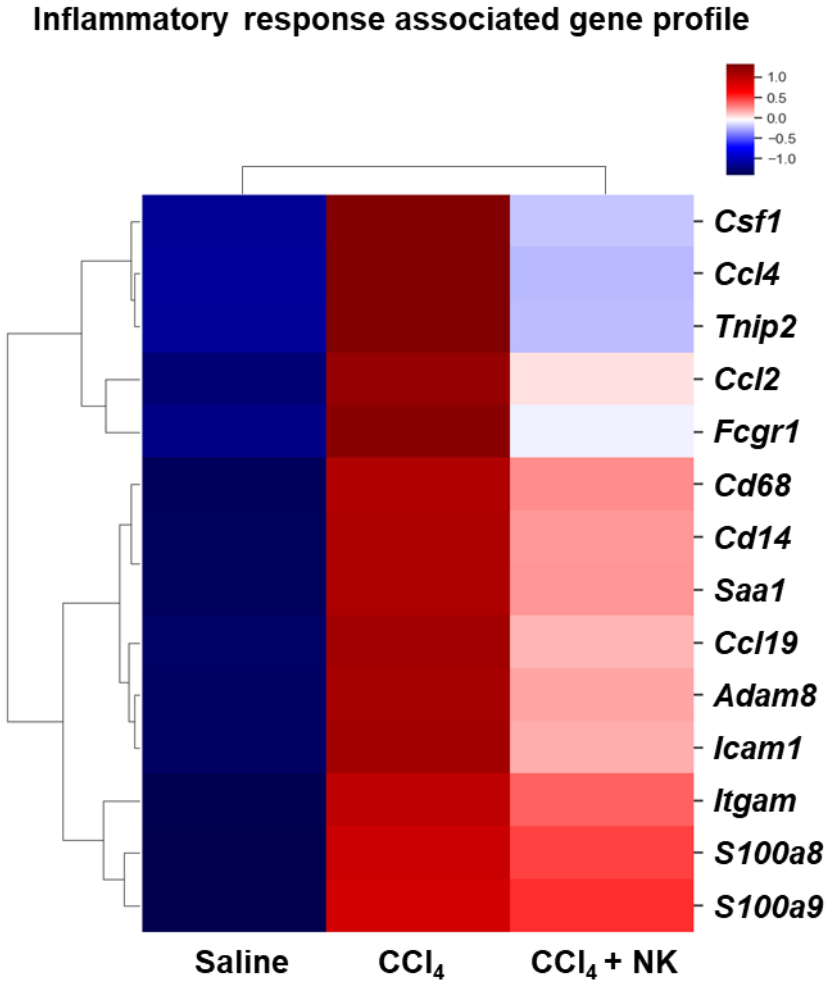
Inflammatory response associated gene profile
1.0
0.5
0.0
−0.5
−1.0
Csf1
Ccl4
Tnip2
Ccl2
Fcgr1
Cd68
Cd14
Saa1
Ccl19
Adam8
Icam1
Itgam
S100a8
S100a9
Saline
CCl4
CCl4 + NK

**B**

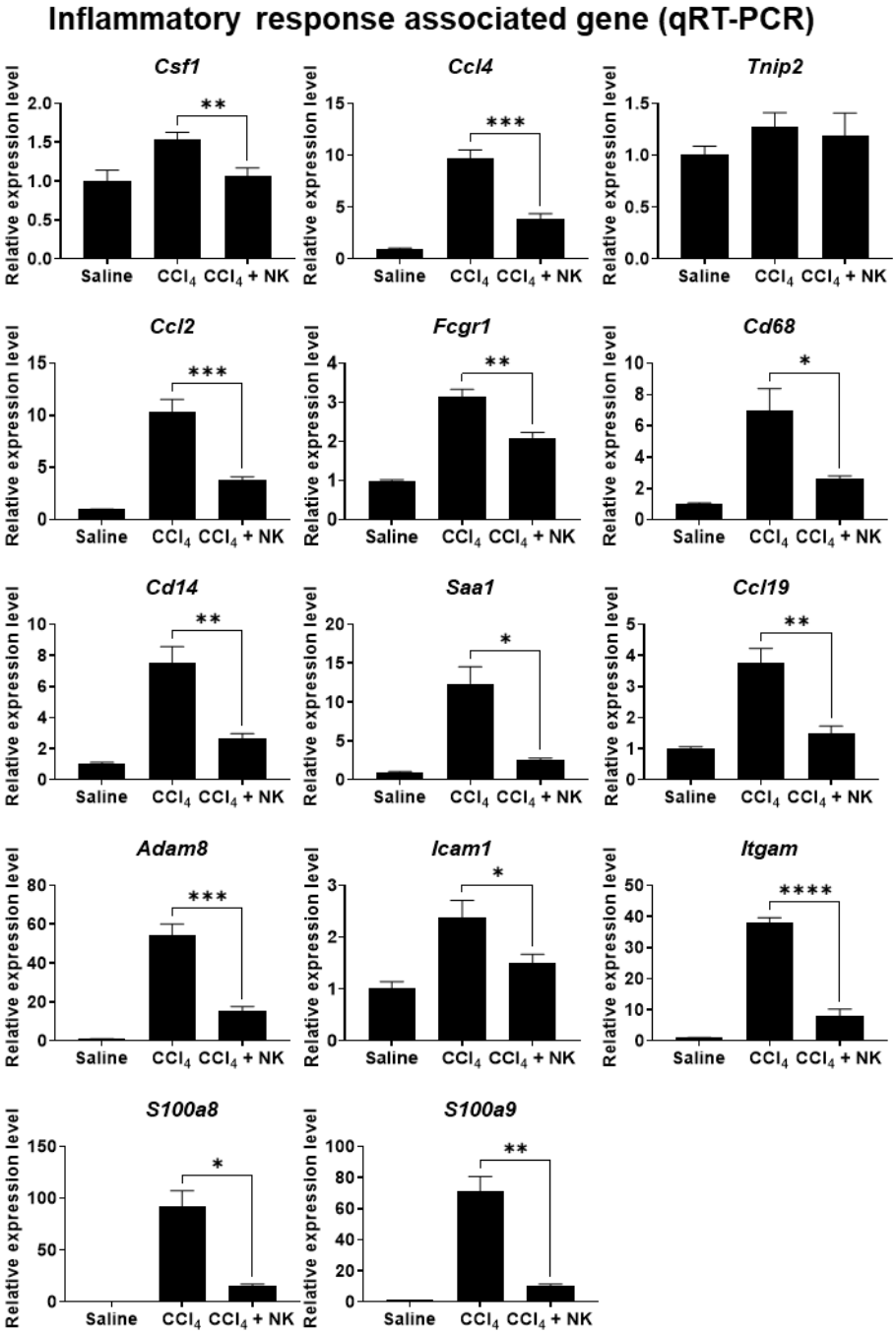
Inflammatory response associated gene (qRT-PCR)
Csf1
Ccl4
Tnip2
Ccl2
Fcgr1
Cd68
Cd14
Saa1
Ccl19
Adam8
Icam1
Itgam
S100a8
S100a9
Relative expression level
Saline
CCl4
CCl4 + NK

Figure 12. Validation of expression levels of DEGs associated with inflammatory response by qRT-PCR

A. Cluster heatmap of upregulated inflammatory response-associated genes (n = 14). The relative gene expression level was indicated by red for high expression and blue for low expression. B. Relative gene expression of inflammatory response-associated genes by qRT-PCR analysis. Data are presented as mean ± SD from three independent experiments. * p-values < 0.05, ** p-values < 0.005, *** p-values < 0.001, and **** p-values < 0.0001.

Taking all the data together, our study on NK cell therapy in a $CCl_4$-induced liver cirrhosis mouse model could be summarized as Figure 13.

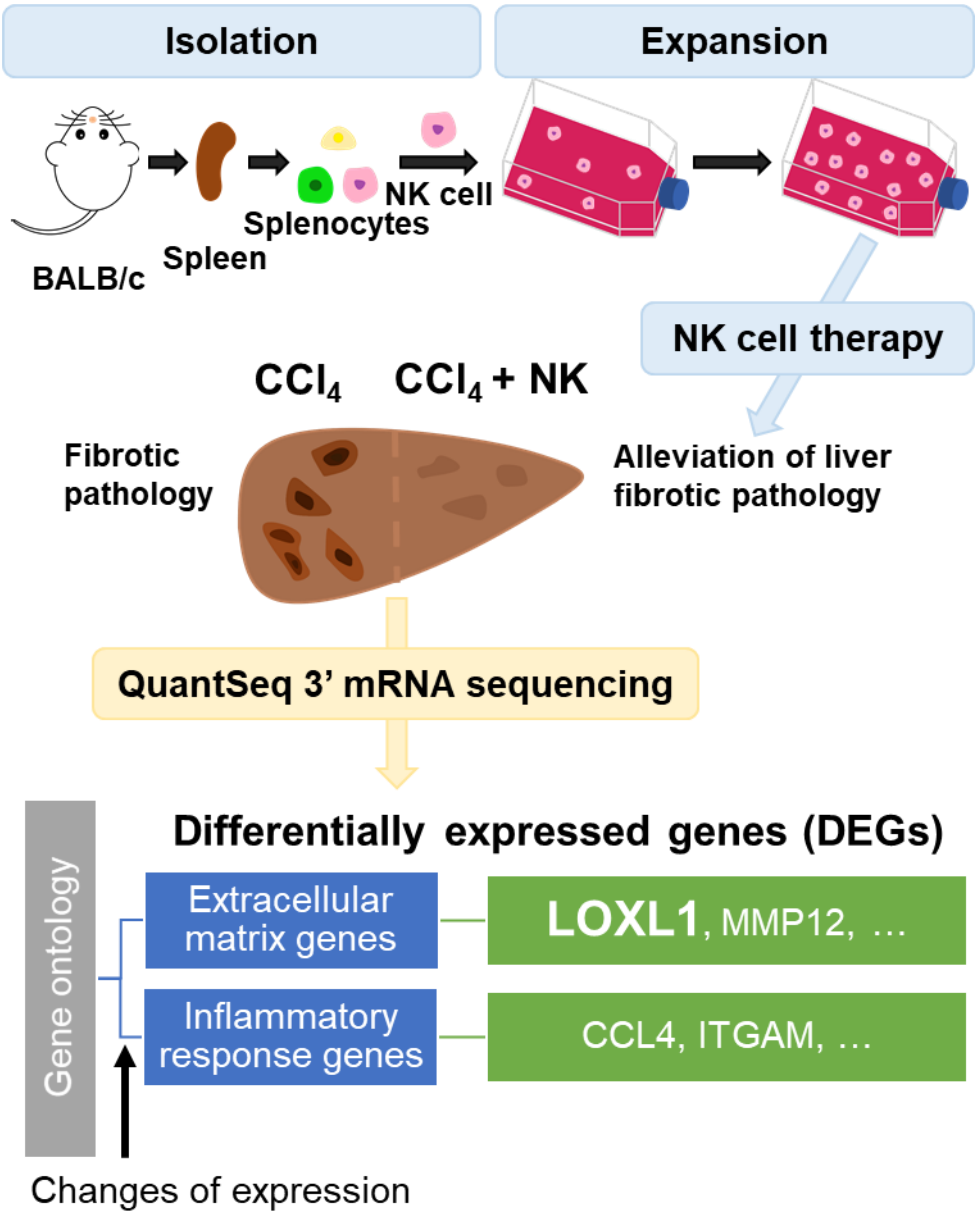


Figure 13. Schematic summary of NK cell therapeutics in $CCl_4$-induced liver cirrhosis mouse model in this study

# Discussion

Previous studies have shown that NK cell functions are suppressed in progressive liver fibrosis [22, 35]. Furthermore, NK cells were reported to have a protective effect against a $CCl_4$-induced-liver cirrhosis mouse model [20-22]. Liver cirrhosis mouse model was used to evaluate the therapeutic potential of NK cell transplantation, which effectively reduced liver fibrotic lesions and cirrhosis progression (Figure 4, 5). The therapeutic potential of NK cell transplantation to decrease key inflammatory factors was investigated, including the cytokine TGF-β1 (Figure 6A), the activated HSC marker α-SMA (Figure 6B). α-SMA is known to be expressed during the activation of HSCs, which occurs when they the activated HSCs produce excessive amounts of fibrillar collagen in response to liver damage [36]. Furthermore, we assessed the influence on F4/80 macrophage infiltration (Figure 6C), which is capable of producing cytokines such as TGF-β1. Finally, the localization of NK cells in the liver of the cirrhotic mice was visualized with BLI (Figure 9A, B).

Current therapeutics for liver cirrhosis can be summarized by several treatment options. One of the considerable therapeutic options is anti-hepatic fibrosis drugs [37]. In addition, gene

therapy, including siRNA and miRNA and cell therapy, could be another therapeutic option for liver cirrhosis [37]. However, because of complicated mechanisms and differences in animal models and patients, drug therapy could lead to poor efficacy [37]. In addition, gene therapy has the strength of providing specificity, but it is essential to exclude systemic unwanted effects. The NK cell therapy is relatively free from these problems and has the advantage of being versatile for various other diseases if specific isolation/expansion is performed as we have proposed. For example, the accumulation of NK cells in the lung was elucidated in the $CCl_4$-induced liver cirrhosis mouse model through the BLI images (Figure 9B), and it could also be applied to additional lung-related studies related to the $CCl_4$-induced liver cirrhosis mouse model.

The therapeutic role of NK cells can only be examined by acquiring sufficient numbers of NK cells. The NK cell frequency in the spleen was reported to be only about 4% of total cells in 2-3-month-old C57BL/6J male mice [25]. Moreover, splenic NK cells were significantly reduced in aged mice (18-19 months old) compared to young mice (2-3 months old) [25]. Even with a nearly 100% acquisition of NK cells from the mouse spleen, multiple mice are needed to obtain about $1 \times 10^7$ NK cells. Therefore, NK cell isolation and expansion method in this study using fewer mice and

allowing for the acquisition of a large number of NK cells for research and therapeutic applications, might be a better alternative. It was reported that there were differences in NK cell receptor expression and IFN-$\gamma$ production in NK cells following IL-2 stimulation according to age and sex [25]. The aged male mice displayed an increased expression of NKG2D in the NK cells compared to young male mice, and young female mice produced significantly more IFN-$\gamma$ than young male mice after 1000 U/mL IL-2 stimulation [25]. High expression of stress ligands by aged cells was reported. It could enhance the expression of its corresponding NKG2D activation receptor in endogenous NK cells. Since aged mice have low NK cell frequency, NK cell supplementation might be beneficial in the aged and diseased liver.

The NK cells that were isolated from the spleen and expanded were mostly CD3e-NKp46+ (>98%) (Figure 2). Just one week of incubation could expand NK cells without significant viability differences (Figure 3B). Moreover, the NK cells exhibited effector functions with a high expression of activation surface markers and a high level of IFN-$\gamma$ secretion (Figure 2, 3C). These results indicated that the expanded NK cells were functional and had typical characteristics of NK cells.

Tracking the location of the immune cells at the target site can

provide important information helpful in elucidating the role of immune cells. A reporter gene imaging technique, BLI, was employed to track NK cells in a cirrhosis mouse model [26]. The transgenic mouse expressing codon-optimized luciferase [28] as a source of NK cells was used to obtain more sensitive luminescence images. The visualization of the NK cells in the cirrhotic liver was important in this study, providing additional evidence for the role of NK cells in the cirrhotic liver.

The accumulation of more NK cells in the liver in the $CCl_4$-induced liver cirrhosis model could be the result of homing to the liver due to chemotaxis of NK cells induced by inflammation in the liver due to $CCl_4$ toxicity [38]. TGF-$\beta$, a representative inflammatory cytokine, has been identified through immunofluorescence staining in a $CCl_4$-induced liver cirrhosis mouse model (Figure 6A). In addition, it was elucidated that chemokines such as *Ccl4* were increased in the $CCl_4$-induced liver cirrhosis mouse model through mRNA sequencing and qRT-PCR (Figure 12A, B).

Relatively low signals were observed in the liver after 36 hours of NK cell inoculation in the control mice, but high signals were observed in the $CCl_4$-induced cirrhotic mice 36 hours after NK cell inoculation (Figure 9A, B). Besides hepatic signals, high pulmonary

signals were simultaneously visualized, requiring a further investigation of their relationship with the lungs (Figure 9B). Accumulation in other organs, such as the heart, kidney, and muscle tissues, was low in both groups (Figure 9A, B).

A recent study reported that CXCL12 paracrine signaling induced liver metastasis by silencing NK cells in activated HSCs in a liver metastasis model of subcutaneous breast cancer [39]. Thus, the interaction between NK cells and HSCs appears to be important in the cancer environment and in the liver cirrhosis model in this study. Therefore, the relationship between the reduction of cirrhosis and NK cells and the specific mechanisms of decreased activated HSC number and the blockade of macrophage infiltration requires further study and is necessary to elucidate the NK cell therapeutic mechanism involved in the liver cirrhosis.

An mRNA transcriptome analysis was conducted on the liver tissue samples obtained from the normal group, the group with induced cirrhosis, and the group treated with NK cells following the induction of cirrhosis. By examining the DEGs in each group, differences were found in the ECM and inflammatory response-related genes (Figure 11A, 12A), which were verified by qRT-PCR (Figure 11B, 12B). These results elucidated that the NK cell-mediated therapeutic effects on liver cirrhosis were related to the

ECM and inflammation (Figure 10-12). The expression levels of the subfamily of MMPs, collagen, and TGF-$\beta$ associated with the fibrotic process were significantly decreased after NK cell treatment (Figure 11). mRNA transcriptomic analysis has revealed that NK cell therapeutic effects in liver cirrhosis models are related to extracellular matrix and inflammation, but it will be necessary to directly identify which mechanism is involved in detail.

Hepatocyte death has been shown to initiate the liver fibrosis pathway [40]. Cellular components released from dead hepatocytes induced HSC activation, proliferation, transformation, and collagen production, leading to fibrosis, cirrhosis, and cancer [41]. HSC activation is known to be induced by platelet-derived growth factor, interleukin (IL)-1, tumor necrosis factor (TNF)-$\alpha$, and others. It was reported that TNF and IL-17 stimulated the differentiation of HSCs into myofibroblast-like cells and induced the expression of $\alpha$-SMA and collagen synthesis through the arginase-proline pathway [42-44].

NK cells are activated by recognizing virus invasion and cancer cells, and they induce immune responses by producing large amounts of TNF-$\alpha$ and IFN-$\gamma$. CD4+ T helper 1 ($T_{h1}$) cells reduce TGF-$\beta$-induced fibrosis-promoting activity through IFN-$\gamma$ secretion and reduce collagen production by suppressing

arginase function via the IFN-$\gamma$-induced JAK/STAT pathway, alleviating fibrosis [21, 43, 45, 46]. It was reported that exosomes derived from NK cells inhibited HSC activation and $CCl_4$-induced hepatic fibrosis [47]. In addition, a recent study reported that the metabotropic glutamate receptor 5 (mGluR5) of NK cells increased IFN-$\gamma$ secretion through the MEK/ERK pathway, suggesting additional cytotoxicity to activated HSCs [48]. The IFN-$\gamma$ secretion was increased about 7.5 times after one week of NK cell expansion, compared to before the expansion (Figure 3C). Taken together, the secretion of IFN-$\gamma$ by NK cells was involved in the alleviation of fibrotic liver pathology.

Furthermore, the mechanism by which NK cells directly kill HSCs might also help alleviate fibrosis. NK cells recognize their target cells through receptors, and stimulatory and inhibitory receptors determine NK cell activation status and their target cell killing effects. The mechanisms of the NK-cell-mediated killing of HSCs was summarized in a review article [41].

Activated HSCs exhibit strong expression of ULBP-2 (UL16 binding protein 2), MICA/B (MHC class I polypeptide-related sequence A/B), and RAE-1 (retinoic acid early inducible 1), which stimulate NK cells by interacting with NKG2D [49-51]. In addition, Activated HSCs express less expression of the NK cell inhibitory

ligand MHC-1 [18]. As a result, NKG2D-dependent degranulation of NK cells leads to the elimination of activated HSCs.

The balance between stimulatory receptors, including NKG2D, NKp30, NKp36, NKp44, and NKp46, and inhibitory receptors, including killer cell immunoglobulin-like receptor (KIR) and Ly49, was reported to be involved in NK cell regulation [52].

In particular, NKG2D and NKp46 are involved in killing HSCs [22, 49, 53, 54]. NKG2D ligands, including retinoic acid-induced early gene 1 (Rae1), MHC class I polypeptide-related sequence A (MICA), and UL16 binding protein (ULBP), are expressed on activated HSCs [22, 49, 53]. NK cells can kill activated HSCs by NKG2D- and tumor necrosis factor-related apoptosis-inducing ligand (TRAIL)-dependent mechanisms [49]. Besides TRAIL, other NK cell surface ligands, including the Fas ligand (FasL), can bind to receptors on HSCs and trigger HSC death through caspase activation and apoptosis [17]. NKp46 also plays a role in triggering lytic activity with its ligand NCR1 [54]. We obtained 61.55 ± 3.47% of NKp46+NKG2D+ NK cells using our expansion method (Figure 2), indicating that the expansion method can retain the killing function of NK cells. In addition, NK cell-mediated HSC cytotoxicity could be induced by the secretion of granules containing perforin and granzyme A/B, which induce HSC apoptosis

[18]. As shown in Figure 2, NKp46+ NK cells (>99%) and NKp46+NKG2D+ NK (61.55 ± 3.47%) cells were investigated in the NK cells. The relationship between cirrhosis and specific subsets of NK cells, such as NKG2D+ NK cells, needs to be further investigated by various methods, including single-cell genomics [55], and might increase the potential of specific cell-based therapeutic techniques [56].

QuantSeq 3′ mRNA sequencing revealed 33 downregulated genes associated with ECM after the NK cell treatment of $CCl_4$-induced cirrhosis, including 6 *Mmp* genes (*Mmp3*, *Mmp8*, *Mmp9*, *Mmp11*, *Mmp12*, and *Mmp14*) (Figure 11). MMPs are a family of extracellular endopeptidases that are thought to be responsible for ECM degradation. For example, MMP2 (gelatinase A) is involved in HSC proliferation and the activation of TGF-$\beta$ [57]. Additionally, MMP2, MMP3, and MMP9 are highly expressed during the acute phase of tissue damage [57], and the role of MMP12 in the treatment of mesenchymal stem cells for liver fibrosis has been reported [58]. Because each specific MMP can perform pro-fibrotic and anti-fibrotic dual functions, the relationship between specific MMPs and NK cell treatment needs to be further investigated.

Furthermore, the involvement of lysyl oxidase-like-1 (*Loxl1*) in

the therapeutic effects of NK cells was demonstrated in the $CCl_4$-induced liver cirrhosis mouse model (Figure 11, Table 2). LOXL1 is one of the lysyl oxidase (LOX) family proteins. The biological functions of LOXL1 are well summarized in a review article [59]. LOXL1 has been reported to be involved in matrix remodeling in the state of injury and subsequently in the fibrosis process, and in particular, increase elastin crosslinking by TGF-$\beta$ signaling [60, 61]. In this study, the increase and decrease of TGF-$\beta$ was evaluated by $CCl_4$-induced liver cirrhosis mouse model and NK cell therapy (Figure 6A, Table 2, Figure 11). Further studies on the regulation of LOXL1 by NK cell therapy are needed. In addition, it was reported that LOXL1 was related to the progression of various tumors, such as glioma, gastric cancer, colorectal cancer, pancreatic ductal adenocarcinoma (PDAC) [62]. However, the association between LOXL1 and liver cancer or pathophysiology has not been well known, however, about a 30-fold increase in the mRNA expression level of *Loxl1* has been reported in a $CCl_4$-induced liver cirrhosis mouse model [63], but the detailed mechanism requires further investigation, and its relation with liver cancer is not well known. Considering the role of LOXL1 in cancer progression, it would be an interesting topic to investigate the role of LOXL1 in liver cancer and the possibility of NK cell therapeutic effects.

QuantSeq 3' mRNA sequencing revealed 41 downregulated genes involved in the inflammatory response including integrin protein – *Itgam*, integrin alpha M, and chemokines - *Csf1*, colony stimulating factor 1, *Ccl2*, Chemokine C–C motif ligand 2, *Ccl4*, Chemokine C–C motif ligand 4, *Ccl19*, Chemokine C–C motif ligand 19.

ITGAM, also known as CD11b, is a cell surface receptor protein that belongs to the integrin family. Integrins are involved in cell adhesion and migration by mediating interactions between cells and extracellular matrix or other cells. CD11b is expressed on various types of macrophages including kupffer cells [64]. It has been reported that the expression of CD11b is related to the fibrosis stage [65]. Further studies are needed on the effect of NK cell therapy on CD11b+ macrophages.

Changes in chemokines such as *Csf1*, *Ccl2*, *Ccl4*, and *Ccl19* were elucidated through RNA sequencing. Chemokines and their receptors play a crucial role in regulating the recruitment of immune cells to damaged or diseased organs [66]. Since chronic inflammation plays an important role in liver fibrosis, the relationship between NK cell therapy and these chemokines will need to be further investigated.

In summary, our results showed that NK cells could function similarly to the original NK cells and had protective effects in the

$CCl_4$-induced liver cirrhosis model. We provided evidence that NK cells could reduce cirrhosis progression by decreasing inflammation and reducing HSC and macrophage numbers in the cirrhotic liver. The therapeutic effects of NK cell transplantation in liver cirrhosis were related to ECM and inflammation. In particular, LOXL1, which has been reported to play an important role in matrix remodeling or fibrosis, was found through mRNA sequencing, and an increase in LOXL1 was elucidated in the $CCl_4$-induced liver cirrhosis model in this study. Thereafter, the reduction of LOXL1 was evaluated during NK cell treatment, and it was elucidated that NK cell treatment was related to LOXL1. Our study suggests that NK cells can potentially be used for therapeutic applications by suppressing inflammation and extracellular matrix-related genes.

# References


1. Schuppan, D., & Afdhal, N.H. (2008). Liver cirrhosis. Lancet, 371(9615), 838-851.
2. Hernandez-Gea, V., & Friedman, S.L. (2011). Pathogenesis of liver fibrosis. Annual Review of Pathology: Mechanisms of Disease, 6, 425-456.
3. Tsuchida, T., & Friedman, S.L. (2017). Mechanisms of hepatic stellate cell activation. Nature Reviews. Gastroenterology & Hepatology, 14(7), 397-411.
4. Coulouarn, C., Corlu, A., Glaise, D., Guénon, I., Thorgeirsson, S.S., & Clément, B. (2012). Hepatocyte-Stellate Cell Cross-Talk in the Liver Engenders a Permissive Inflammatory Microenvironment That Drives Progression in Hepatocellular Carcinoma. Cancer Research, 72(10), 2533-2542.
5. Carloni, V., Luong, T.V., & Rombouts, K. (2014). Hepatic stellate cells and extracellular matrix in hepatocellular carcinoma: More complicated than ever. Liver International, 34(6), 834-843.
6. Novikova, M., Khromova, N., & Kopnin, P. (2017). Components of the hepatocellular carcinoma microenvironment and their role in tumor progression. Biochemistry, 82(8),

861-873.

7. Amarapurkar, D.N. (2011). Prescribing medications in patients with decompensated liver cirrhosis. International Journal of Hepatology, 2011, 519526.

8. Zhou, W.-C., Zhang, Q.-B., & Qiao, L. (2014). Pathogenesis of liver cirrhosis. World Journal of Gastroenterology, 20(23), 7312-7324.

9. Scholten, D., Trebicka, J., Liedtke, C., & Weiskirchen, R. (2015). The carbon tetrachloride model in mice. Laboratory Animals, 49(1_suppl), 4-11.

10. Chen, X., Zhang, J., Yi, R., Mu, J., Zhao, X., & Yang, Z. (2018). Hepatoprotective effects of Lactobacillus on carbon tetrachloride-induced acute liver injury in mice. International Journal of Molecular Sciences, 19(8), 2212.

11. Eom, Y.W., Shim, K.Y., & Baik, S.K. (2015). Mesenchymal stem cell therapy for liver fibrosis. Korean Journal of Internal Medicine, 30(5), 580.

12. Cho, K.A., Ju, S.Y., Cho, S.J., Jung, Y.J., Woo, S.Y., Seoh, J.Y., Han, H.S., & Ryu, K.H. (2009). Mesenchymal stem cells showed the highest potential for the regeneration of injured liver tissue compared with other subpopulations of the bone marrow. Cell Biology International, 33(7), 772-777.

13. Eom, Y.W., Kim, G., & Baik, S.K. (2015). Mesenchymal stem cell therapy for cirrhosis: Present and future perspectives. World Journal of Gastroenterology, 21(34), 10253.

14. Fasbender, F., Widera, A., Hengstler, J.G., & Watzl, C. (2016). Natural killer cells and liver fibrosis. Frontiers in Immunology, 7, 19.

15. Liu, P., Chen, L., & Zhang, H. (2018). Natural killer cells in liver disease and hepatocellular carcinoma and the NK cell-based immunotherapy. Journal of Immunology Research, 2018, 1206737.

16. Gao, B., Jeong, W.I., & Tian, Z. (2008). Liver: An organ with predominant innate immunity. Hepatology, 47(2), 729-736.

17. Notas, G., Kisseleva, T., & Brenner, D. (2009). NK and NKT cells in liver injury and fibrosis. Clinical Immunology, 130(1), 16-26.

18. Melhem, A., Muhanna, N., Bishara, A., Alvarez, C.E., Ilan, Y., Bishara, T., Horani, A., Nassar, M., Friedman, S.L., & Safadi, R. (2006). Anti-fibrotic activity of NK cells in experimental liver injury through killing of activated HSC. Journal of Hepatology, 45(1), 60-71.

19. Radaeva, S., Wang, L., Radaev, S., Jeong, W.I., Park, O., & Gao, B. (2007). Retinoic acid signaling sensitizes hepatic stellate

cells to NK cell killing via upregulation of NK cell activating ligand RAE1. American Journal of Physiology. Gastrointestinal and Liver Physiology, 293(4), G809-G816.

20. Gao, B., Radaeva, S., & Jeong, W.I. (2007). Activation of natural killer cells inhibits liver fibrosis: A novel strategy to treat liver fibrosis. Expert Review of Gastroenterology & Hepatology, 1(2), 173-180.

21. Jeong, W.I., Park, O., Radaeva, S., & Gao, B. (2006). STAT1 inhibits liver fibrosis in mice by inhibiting stellate cell proliferation and stimulating NK cell cytotoxicity. Hepatology, 44(5), 1441-1451.

22. Jeong, W.I., Park, O., Suh, Y.G., Byun, J.S., Park, S.Y., Choi, E., Kim, J.K., Ko, H., Wang, H., & Miller, A.M. (2011). Suppression of innate immunity (natural killer cell/interferon-$\gamma$) in the advanced stages of liver fibrosis in mice. Hepatology, 53(4), 1342-1351.

23. Li, X., Zhang, M., Liu, J., Huang, Z., Zhao, Q., Huang, Y., Li, X., & Gao, Z. (2016). Intrahepatic NK cells function suppressed in advanced liver fibrosis. European Journal of Clinical Investigation, 46(10), 864-872.

24. Yi, H.S., & Jeong, W.I. (2013). Interaction of hepatic stellate cells with diverse types of immune cells: Foe or friend?

Journal of Gastroenterology and Hepatology, 28(1), 99-104.

25. Menees, K.B., Earls, R.H., Chung, J., Jernigan, J., Filipov, N.M., Carpenter, J.M., & Lee, J.-K. (2021). Sex- and age-dependent alterations of splenic immune cell profile and NK cell phenotypes and function in C57BL/6J mice. Immunity & Ageing, 18, 1-13.
26. Youn, H., & Chung, J.-K. (2013). Reporter gene imaging. American Journal of Roentgenology, 201(4), W206-W214.
27. Youn, H., & Hong, K.-J. (2019). Non-invasive molecular imaging of immune cell dynamics for vaccine research. Clinical and Experimental Vaccine Research, 8(2), 89-93.
28. Rabinovich, B.A., Ye, Y., Etto, T., Chen, J.Q., Levitsky, H.I., Overwijk, W.W., Cooper, L.J., Gelovani, J., & Hwu, P. (2008). Visualizing fewer than 10 mouse T cells with an enhanced firefly luciferase in immunocompetent mouse models of cancer. Proceedings of the National Academy of Sciences of the United States of America, 105(38), 14342-14346.
29. Ozsolak, F., & Milos, P.M. (2011). RNA sequencing: Advances, challenges and opportunities. Nature Reviews Genetics, 12(2), 87-98.
30. Stark, R., Grzelak, M., & Hadfield, J. (2019). RNA sequencing: The teenage years. Nature Reviews Genetics, 20(11), 631-

656.

31. Wang, G., Yu, G., Wang, D., Guo, S., & Shan, F. (2017). Comparison of the purity and vitality of natural killer cells with different isolation kits. Experimental and Therapeutic Medicine, 13, 1875-1883.

32. Yang, N., Ko, M., Ahn, M., & Shin, T. (2023). Hepatoprotective effects of norgalanthamine on carbon tetrachloride induced-hepatotoxicity in mice. Drug and Chemical Toxicology, 46(2), 144-154.

33. Langmead, B., & Salzberg, S.L. (2012). Fast gapped-read alignment with Bowtie 2. Nature Methods, 9(4), 357-359.

34. Quinlan, A.R., & Hall, I.M. (2010). BEDTools: A flexible suite of utilities for comparing genomic features. Bioinformatics, 26(6), 841-842.

35. Lee, Y.S., & Jeong, W.I. (2012). Retinoic acids and hepatic stellate cells in liver disease. Journal of Gastroenterology and Hepatology, 27(1), 75-79.

36. Carpino, G., Morini, S., Corradini, S. G., Franchitto, A., Merli, M., Siciliano, M., ... & Gaudio, E. (2005). Alpha-SMA expression in hepatic stellate cells and quantitative analysis of hepatic fibrosis in cirrhosis and in recurrent chronic hepatitis after liver transplantation. Digestive and Liver Disease, 37(5),

349-356.

37. Tan, Z., Sun, H., Xue, T., Gan, C., Liu, H., Xie, Y., Yao, Y., & Ye, T. (2021). Liver fibrosis: Therapeutic targets and advances in drug therapy. Frontiers in Cell and Developmental Biology, 9, 730176.

38. Ran, G. H., Lin, Y. Q., Tian, L., Zhang, T., Yan, D. M., Yu, J. H., & Deng, Y. C. (2022). Natural killer cell homing and trafficking in tissues and tumors: from biology to application. Signal Transduction and Targeted Therapy, 7(1), 205.

39. Correia, A.L., Guimaraes, J.C., Auf der Maur, P., De Silva, D., Trefny, M.P., Okamoto, R., Bruno, S., Schmidt, A., Mertz, K., & Volkmann, K. (2021). Hepatic stellate cells suppress NK cell-sustained breast cancer dormancy. Nature, 594(7861), 566-571.

40. Mehal, W., & Imaeda, A. (2010). Cell death and fibrogenesis. Seminars in Liver Disease, 30(3), 226-231.

41. Wei, Y., Bingyu, W., Lei, Y., & Xingxing, Y. (2022). The antifibrotic role of natural killer cells in liver fibrosis. Experimental Biology and Medicine, 247(11), 1235-1243.

42. Parola, M., & Pinzani, M. (2019). Liver fibrosis: Pathophysiology, pathogenetic targets and clinical issues. Molecular Aspects of Medicine, 65, 37-55.

43. Wree, A., McGeough, M.D., Inzaugarat, M.E., Eguchi, A., Schuster, S., Johnson, C.D., Peña, C.A., Geisler, L.J., Papouchado, B.G., Hoffman, H.M., et al. (2018). NLRP3 inflammasome driven liver injury and fibrosis: Roles of IL-17 and TNF in mice. Hepatology, 67(2), 736-749.

44. Szondi, D.C., Wong, J.K., Vardy, L.A., & Cruickshank, S.M. (2021). Arginase signalling as a key player in chronic wound pathophysiology and healing. Frontiers in Molecular Biosciences, 8, 1049.

45. Stark, G.R., Kerr, I.M., Williams, B.R., Silverman, R.H., & Schreiber, R.D. (1998). How cells respond to interferons. Annual Review of Biochemistry, 67, 227-264.

46. Wynn, T.A., & Ramalingam, T.R. (2012). Mechanisms of fibrosis: Therapeutic translation for fibrotic disease. Nature Medicine, 18(7), 1028-1040.

47. Wang, L., Wang, Y., & Quan, J. (2020). Exosomes derived from natural killer cells inhibit hepatic stellate cell activation and liver fibrosis. Human Cell, 33(2), 582-589.

48. Choi, W.M., Ryu, T., Lee, J.H., Shim, Y.R., Kim, M.H., Kim, H.H., Kim, Y.E., Yang, K., Kim, K., Choi, S.E., et al. (2021). Metabotropic glutamate receptor 5 in natural killer cells attenuates liver fibrosis by exerting cytotoxicity to activated

stellate cells. Hepatology, 74(4), 2170-2185.

49. Radaeva, S., Sun, R., Jaruga, B., Nguyen, V. T., Tian, Z., & Gao, B. (2006). Natural killer cells ameliorate liver fibrosis by killing activated stellate cells in nkg2d-dependent and tumor necrosis factor–related apoptosis-inducing ligand–dependent manners. Gastroenterology, 130(2), 435-452.

50. Glässner, A., Eisenhardt, M., Krämer, B., Körner, C., Coenen, M., Sauerbruch, T., ... & Nattermann, J. (2012). NK cells from HCV-infected patients effectively induce apoptosis of activated primary human hepatic stellate cells in a TRAIL-, FasL-and NKG2D-dependent manner. Laboratory Investigation, 92(7), 967-977.

51. Mitra, A., Satelli, A., Yan, J., Xueqing, X., Gagea, M., Hunter, C. A., ... & Li, S. (2014). IL-30 (IL27p28) attenuates liver fibrosis through inducing NKG2D-rae1 interaction between NKT and activated hepatic stellate cells in mice. Hepatology, 60(6), 2027-2039.

52. Pegram, H.J., Andrews, D.M., Smyth, M.J., Darcy, P.K., & Kershaw, M.H. (2011). Activating and inhibitory receptors of natural killer cells. Immunology and Cell Biology, 89(2), 216-224.

53. Krizhanovsky, V., Yon, M., Dickins, R.A., Hearn, S., Simon, J.,

Miething, C., Yee, H., Zender, L., & Lowe, S.W. (2008). Senescence of activated stellate cells limits liver fibrosis. Cell, 134(4), 657-667.

54. Gur, C., Doron, S., Kfir-Erenfeld, S., Horwitz, E., Abu-Tair, L., Safadi, R., & Mandelboim, O. (2012). NKp46-mediated killing of human and mouse hepatic stellate cells attenuates liver fibrosis. Gut, 61(6), 885-893.

55. Ren, C., Li, M., Zheng, Y., Cai, B., Du, W., Zhang, H., Wu, F., Tong, M., Lin, F., & Wang, J. (2022). Single-cell RNA-seq reveals altered NK cell subsets and reduced levels of cytotoxic molecules in patients with ankylosing spondylitis. Journal of Cellular and Molecular Medicine, 26(2), 1071-1082.

56. Mount, N.M., Ward, S.J., Kefalas, P., & Hyllner, J. (2015). Cell-based therapy technology classifications and translational challenges. Philosophical Transactions of the Royal Society B: Biological Sciences, 370(1680), 20150017.

57. Khurana, A., Sayed, N., Allawadhi, P., & Weiskirchen, R. (2021). It's all about the spaces between cells: Role of extracellular matrix in liver fibrosis. Annals of Translational Medicine, 9(21), 728.

58. Wang, M., Zhang, M., Fu, L., Lin, J., Zhou, X., Zhou, P., Huang, P., Hu, H., & Han, Y. (2020). Liver-targeted delivery of

TSG-6 by calcium phosphate nanoparticles for the management of liver fibrosis. Theranostics, 10(1), 36.

59. Greene, A. G., Eivers, S. B., Dervan, E. W., O'Brien, C. J., & Wallace, D. M. (2020). Lysyl oxidase like 1: biological roles and regulation. Experimental eye research, 193, 107975.

60. Zhao, W., Yang, A., Chen, W., Wang, P., Liu, T., Cong, M., ... & You, H. (2018). Inhibition of lysyl oxidase-like 1 (LOXL1) expression arrests liver fibrosis progression in cirrhosis by reducing elastin crosslinking. Biochimica et Biophysica Acta (BBA)-Molecular Basis of Disease, 1864(4), 1129-1137.

61. Ma, L., Zeng, Y., Wei, J., Yang, D., Ding, G., Liu, J., ... & Ji, X. (2018). Knockdown of LOXL1 inhibits TGF-β1-induced proliferation and fibrogenesis of hepatic stellate cells by inhibition of Smad2/3 phosphorylation. Biomedicine & Pharmacotherapy, 107, 1728-1735.

62. Lin, H.-Y., Li, C.-J., Yang, Y.-L., Huang, Y.-H., Hsiau, Y.-T., & Chu, P.-Y. (2020). Roles of lysyl oxidase family members in the tumor microenvironment and progression of liver cancer. International Journal of Molecular Sciences, 21(24), 9751.

63. Zhao, W., Yang, A., Chen, W., Wang, P., Liu, T., Cong, M., Xu, A., Yan, X., Jia, J., & You, H. (2018). Inhibition of lysyl oxidase-like 1 (LOXL1) expression arrests liver fibrosis

progression in cirrhosis by reducing elastin crosslinking. Biochimica et Biophysica Acta (BBA) - Molecular Basis of Disease, 1864(4), 1129-1137.

64. Ikarashi, M., Nakashima, H., Kinoshita, M., Sato, A., Nakashima, M., Miyazaki, H., Nishiyama, K., Yamamoto, J., & Seki, S. (2013). Distinct development and functions of resident and recruited liver Kupffer cells/macrophages. Journal of Leukocyte Biology, 94(6), 1325-1336.

65. Sanchez, J.I., Parra, E.R., Jiao, J., Solis Soto, L.M., Ledesma, D.A., & Beretta, L. (2023). Cellular and Molecular Mechanisms of Liver Fibrosis in Patients with NAFLD. Cancers, 15(11), 2871.

66. Marra, F., & Tacke, F. (2014). Roles for chemokines in liver disease. Gastroenterology, 147(3), 577-594.

# 국문 초록

만성 간 질환은 간섬유증, 간경변 및/또는 간암을 유도할 수 있으며, 이는 전 세계적인 질병 및 사망의 주요 원인이다. 활성화된 간성상세포는 간섬유증 진행에 악영향을 미치는 것으로 알려져 있다. 자연살해세포는 수용체 활성화를 통해 비정상 또는 형질전환 세포를 선택적으로 인식하고 표적 세포 사멸을 유도하는 것으로 알려져 있어 간경변에 대한 잠재적인 치료 전략으로 사용될 수 있다. 본 연구에서는 사염화탄소로 유발된 간경변 마우스 모델에서 자연살해세포의 치료 효과를 조사하였다.

자연살해세포를 비장에서 분리하고 사이토카인으로 자극한 배양 배지에서 증식시켰다. Natural killer group 2, member D (NKG2D) 양성 자연살해세포는 배양 7일 후에 유의하게 증가하였다. 이러한 자연살해세포의 반복적인 정맥 주사를 통해 콜라겐 침착, 간성상세포 활성 및 대식세포의 침윤을 감소시켜 간경변을 효과적으로 완화하였다. 생체 내에서 자연살해세포를 추적하기 위해, 루시퍼레이스 발현 자연살해세포를 코돈 최적화된 루시페레이스 발현 형질전환 마우스로부터 분리 및 증식시켜 간경변 마우스 모델에 투여하였다. 생물발광 이미징을 통해 간경변 간에서 주입된 자연살해세포의 축적이 나타남을 확인하였다. 또한 QuantSeq 3' mRNA 시퀀싱 기반 전사체 분석을 수행하여 1532개의 차등 발현 유전자에서 자연살해세포 치료 간경변 조직에서 세포외기질에서 33개의 하향 조절된 유전자와 염증 반응에 관련된 41개의 하향 조절된 유전자를 식별하였다. 이 결과로부터 사염화탄소로 유발된 간경변 마우스 모델

에서 자연살해세포의 반복 투여가 항섬유증 및 항염증 기전을 통해 간 섬유화 병리를 완화함을 나타냈다. 종합하면, 이번 연구를 통해 자연살해세포가 사염화탄소 유발 간경변 마우스 모델에서 치료 효과를 가질 수 있음을 입증하였다. 특히 자연살해세포 치료 시 주로 영향을 받은 세포 외기질 유전자와 염증 반응 유전자가 잠재적 표적이 될 수 있음을 밝혀내었다.